Outbursts of the intermediate-mass black hole HLX-1: a wind-instability scenario

Roberto Soria,[1,2,3]★ Aina Musaeva,[2] Kinwah Wu,[4] Luca Zampieri,[5]★ Sara Federle,[5] Ryan Urquhart,[1] Edwin van der Helm[6] and Sean Farrell[2]

[1]*International Centre for Radio Astronomy Research, Curtin University, GPO Box U1987, Perth, WA 6845, Australia*
[2]*Sydney Institute for Astronomy, School of Physics A28, The University of Sydney, Sydney, NSW 2006, Australia*
[3]*National Astronomical Observatories, Chinese Academy of Sciences, Beijing 100012, China*
[4]*Mullard Space Science Laboratory, University College London, Holmbury St. Mary, Dorking, Surrey, RH5 6NT, UK*
[5]*INAF, Astronomical Observatory of Padova, vicolo dell'Osservatorio 5, I-35122 Padova, Italy*
[6]*Leiden Observatory, Leiden University, PO Box 9513, NL-2300 RA Leiden, the Netherlands*

ABSTRACT

We model the intermediate-mass black hole HLX-1, using the *Hubble Space Telescope*, *XMM–Newton* and *Swift*. We quantify the relative contributions of a bluer component, function of X-ray irradiation, and a redder component, constant and likely coming from an old stellar population. We estimate a black hole mass $\approx(2^{+2}_{-1}) \times 10^4 \, \mathrm{M_{\odot}}$, a spin parameter $a/M \approx 0.9$ for moderately face-on view and a peak outburst luminosity ≈ 0.3 times the Eddington luminosity. We discuss the discrepancy between the characteristic sizes inferred from the short X-ray time-scale ($R \sim$ a few 10^{11} cm) and from the optical emitter ($R\sqrt{\cos\theta} \approx 2.2 \times 10^{13}$ cm). One possibility is that the optical emitter is a circumbinary disc; however, we disfavour this scenario because it would require a very small donor star. A more plausible scenario is that the disc is large but only the inner annuli are involved in the X-ray outburst. We propose that the recurrent outbursts are caused by an accretion-rate oscillation driven by wind instability in the inner disc. We argue that the system has a long-term-average accretion rate of a few per cent Eddington, just below the upper limit of the low/hard state; a wind-driven oscillation can trigger transitions to the high/soft state, with a recurrence period $\sim$1 yr (much longer than the binary period, which we estimate as $\sim$10 d). The oscillation that dominated the system in the last decade is now damped such that the accretion rate no longer reaches the level required to trigger a transition. Finally, we highlight similarities between disc winds in HLX-1 and in the Galactic black hole V404 Cyg.

Key words: black hole physics – X-rays: binaries – X-rays: individual: HLX-1.

1 INTRODUCTION

The transient X-ray source HLX-1 (Farrell et al. 2009b) is arguably the most convincing off-nuclear intermediate-mass black hole (IMBH) candidate. The X-ray source is unambiguously associated with an Hα-emitting optical counterpart, providing a recession speed of $\approx$7100 km s^{-1} (Wiersema et al. 2010; Soria, Hau & Pakull 2013); this is consistent with the recession velocity of the surrounding galaxy cluster Abell 2877 (Malumuth et al. 1992). HLX-1 is projected in front of the halo of the S0 galaxy ESO 243-49 (a member of Abell 2877), $\approx$7 arcsec from its nucleus (Fig. 1), which

has a systemic recession speed of $\approx$6700 km s^{-1}. For this reason, we assume the same luminosity distance $\approx$92 Mpc for both ESO 243-49 and HLX-1 (NASA/IPAC Extragalactic Database). It is unclear whether HLX-1 is orbiting around ESO 243-49 or it is simply a chance association within Abell 2877; in either case, HLX-1 is not a foreground Galactic object. If we assume isotropic emission, the peak X-ray luminosity in each of its six fully monitored outbursts is $L_X \approx (1\text{--}1.5) \times 10^{42}$ erg s^{-1} (Yan et al. 2015), corresponding to the Eddington luminosity of a $10^4 \, \mathrm{M_{\odot}}$ BH. At outburst peak, the X-ray spectrum is well fitted with a radiatively efficient, multicolour disc model (Davis et al. 2011; Farrell et al. 2012; Godet et al. 2012), typical of accreting BHs in the sub-Eddington high/soft state. The peak colour temperature ($kT_{in} \approx 0.25$ keV) and the inner radius of the disc ($R_{in}\sqrt{\cos\theta} \sim 5\text{--}10 \times 10^4$ km) are self-consistent with a $\sim 10^4 \, \mathrm{M_{\odot}}$ BH accreting just below its Eddington limit (Godet et al. 2012). The

★ E-mail: roberto.soria@curtin.edu.au (RS); luca.zampieri@oapd.inaf.it (LZ)

Figure 1. HLX-1 appears as a point-like blue source (marked by an arrow) projected in front of the galaxy ESO 243-49. Top panel: *HST*/WFC3 image from 2010 September 23 (absolute brightness $M_V \approx -11$ mag); red corresponds to the *F775W* filter, green to the *F555W* filter and blue to the *F300X* filter. Bottom panel: same as in the top panel, for the 2013 July 5 image (absolute brightness $M_V \approx -10$ mag). In both images, north is up and east to the left.

low rms variability is also consistent with an accretion disc in the high/soft state (Servillat et al. 2011). The outburst evolution after the peak is similar to that of sub-Eddington Galactic BHs: in the first few weeks, a power-law tail appears, strengthens and becomes flatter, while the disc component evolves to lower luminosities and temperatures along the characteristic $L \propto T_{in}^4$ track (Servillat et al. 2011; Godet et al. 2012). In each of its six fully recorded outbursts (Fig. 2), after ~100–150 d and after it declined to a luminosity $\lesssim 10^{41}$ erg s^{-1}, HLX-1 underwent a transition to the low/hard state, with a spectrum dominated by a power law of photon index $\Gamma = 1.6 \pm 0.3$ (Servillat et al. 2011; Yan et al. 2015). The detection of transient radio emission during an outburst (Webb et al. 2012) and the presence of a jet in the low/hard state (Cseh et al. 2015) also support the interpretation that HLX-1 cycles through the canonical states of an accreting BH, with radio flaring generally observed between the hard outburst rise and the transition to the thermal dominant state (Fender, Belloni & Gallo 2004).

Despite the success of this IMBH model based on canonical sub-Eddington accretion states, several questions remain unanswered; failure to solve such problems might even lead to a rejection of the canonical IMBH model, in favour for example of a beamed, highly super-Eddington stellar-mass BH (Lasota, King & Dubus 2015). The main outstanding problems are as follows:
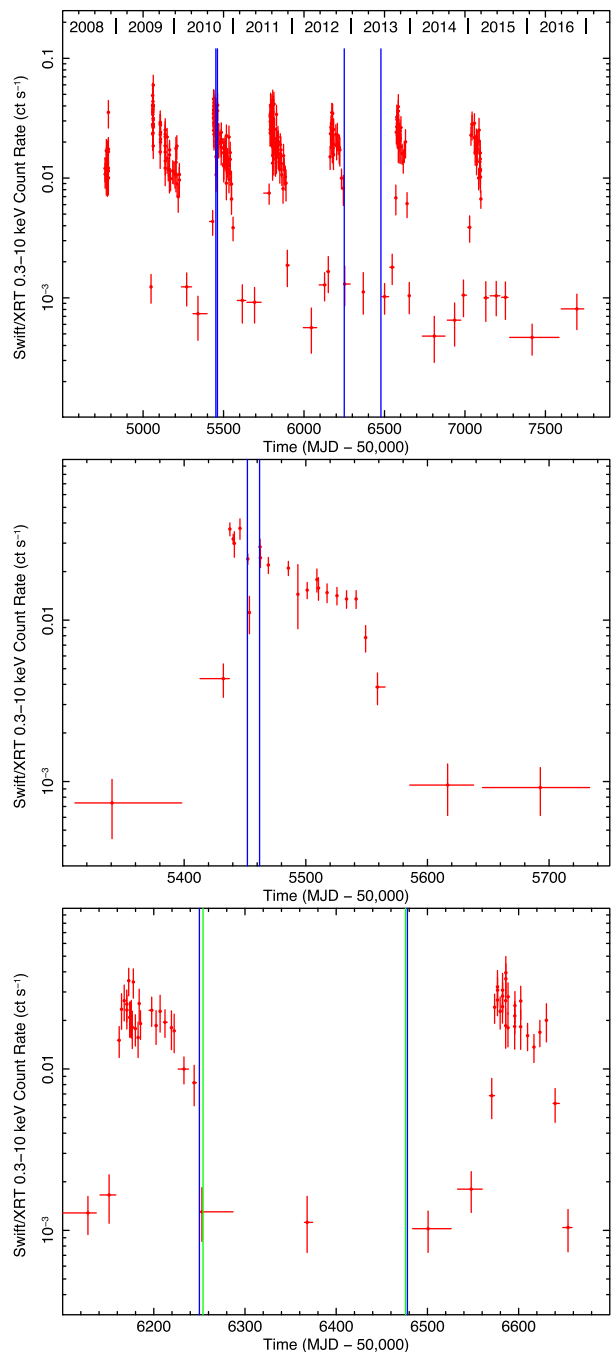
Figure 2. Top panel: *Swift*/XRT snapshot light curve in the 0.3–10 keV band, binned by signal-to-noise >3 (updated to the end of 2016). Blue vertical lines mark the epochs of the *HST* observations. Middle panel: zoomed-in view of the 2010 outburst, binned by XRT observation and signal-to-noise >3. Bottom panel: same for the 2012 and 2013 outbursts; blue lines are the *HST* observations and green lines are the two *XMM–Newton* observations discussed in this work.

(i) What component of the optical/UV luminosity comes from the irradiated accretion disc (variable component) and what from a surrounding star cluster (constant component)?

(ii) What is the size of the accretion disc and of the semi-major axis of the binary system? More specifically, can the accretion disc be small enough to explain the short outburst time-scale but at the same time large enough to produce the observed optical luminosity?

(iii) What causes the repeated outburst behaviour and determines the recurrence time-scale: thermal-viscous instability, periastron passages, other types of mass transfer instabilities, oscillations induced by radiation pressure or outflows?

In this paper, we will discuss those sets of questions, re-examine published and unpublished observational results, and propose a new scenario that may be consistent with all the data. We will determine the BH mass and other system parameters consistent with this scenario.

2 OPTICAL/UV AND X-RAY STUDY

2.1 Setting the problem: distinguishing accretion disc and stellar contributions

The point-like optical source discovered at the position of HLX-1 (Soria et al. 2010), in a region devoid of any other bright X-ray or optical point-like sources, might in principle be a chance coincidence, rather than being physically associated with the hyperluminous X-ray source. If it were a chance association, the detection of a redshifted Hα emission line from the optical counterpart (Wiersema et al. 2010; Soria et al. 2013) suggests that the optical source is at ≈100 Mpc while the X-ray source might be a lower luminosity foreground X-ray binary. This is statistically implausible, and would also make the disc temperature and luminosity of HLX-1 no longer consistent with canonical BH accretion states (Farrell et al. 2009b; Yan et al. 2015). Further strong evidence of a physical connection between X-ray and optical emission comes from their variability properties, as discussed below.

The physical interpretation of the optical/UV emission has been a topic of intense debate. The source is too bright ($M_V \approx -11$ mag in outburst; Farrell et al. 2012) to be an individual O star or even a group of few O stars. Two alternative possibilities were proposed (Farrell et al. 2012; Soria et al. 2012a), based on combined fits of the X-ray and optical/UV spectrum in outburst: either the optical emission is dominated by a young, massive ($M_* \sim 10^6 \, M_\odot$) star cluster or it comes mostly from the X-ray-irradiated accretion disc, supplemented by an older stellar population (age >10 Gyr) to account for an observed near-infrared (near-IR) excess.

Different formation and evolution scenarios for the candidate IMBH are supported by either interpretation of the optical counterpart. If most of the near-UV and blue emission is from a young star cluster, a recent, localized episode of intense star formation is required. There is no other evidence of recent star formation in the halo of ESO 243-49, but the young cluster could be the nucleus of a recently accreted gas-rich dwarf galaxy (Farrell et al. 2012; Mapelli, Zampieri & Mayer 2012; Mapelli et al. 2013a,b). A young, massive star cluster could be a suitable location for the formation and growth of an IMBH (Portegies Zwart & McMillan 2002; Gürkan, Freitag & Rasio 2004). Instead, if the near-UV and blue light is mostly reprocessed thermal emission from an irradiated accretion disc, there is much less need for a massive supply of gas and substantial recent star formation in the star cluster. If the donor star is a red giant or asymptotic giant branch star, or a blue straggler, the cluster may consist entirely of an old population; alternatively, the cluster may contain a few young, massive stars near the centre (including the IMBH donor), perhaps formed from a small amount of gas swept up from the interstellar medium (Conroy & Spergel 2011; Li et al. 2016). Moreover, if the near-UV and blue emission turn out to be from the irradiated disc, we can use that observed flux

to obtain a characteristic size of the emitting region, and from that constrain the size of the BH Roche lobe and the binary separation.

In the young cluster scenario, the optical/UV emission is not expected to show substantial variations on time-scales shorter than the evolution or the dynamical time-scale of the cluster. In the irradiated disc scenario, brightness variations in X-rays and optical are naturally expected, as a system could get into an outburst phase or retreat into quiescence. Very Large Telescope (VLT) observations taken just before and during the rise of the 2012 outburst showed an increase in the visual brightness of $\Delta V = 1.8 \pm 0.4$ mag between near-quiescence (365 d after the peak of the previous outburst) and outburst peak (Webb et al. 2014). In the *R* band, a comparison of observations taken with the *Hubble Space Telescope* (*HST*), VLT, Gemini and Magellan at different times over 2009–2012 suggests a brightness change of $\Delta R = 0.9 \pm 0.4$ mag between outburst and quiescence (Farrell et al. 2014; Webb et al. 2014); however, this result may be affected by systematic errors in the conversion between different filter bands. Moreover, the diffuse emission from the old (red) stellar population in the halo of ESO 243-49 substantially reduces the detection significance of the HLX-1 counterpart from ground-based telescopes, especially towards quiescence.

2.2 *HST*, *XMM–Newton* and *Swift* data analysis

In this work, we present and compare the photometric results from three sets of *HST* observations, taken with the Wide Field Camera 3 (WFC3; UVIS and IR apertures), on 2010 September 23 (≈16 d after outburst peak), on 2012 November 19 (≈72 d after peak) and on 2013 July 5–6 (≈300 d after peak; Table 1). Ultraviolet observations were also taken on 2010 September 13, 2012 November 19 and 2013 July 5 with the Advanced Camera for Surveys Solar Blind Channel (ACS SBC). To model the optical/UV data, we fit them simultaneously with representative X-ray spectra taken as close as possible to the optical observations, and/or at a similar level of X-ray luminosity. For the 2012 *HST* data, we used a 54 ks *XMM–Newton* observation taken on November 23. For the 2013 *HST* data, we used a 141 ks *XMM–Newton* observation taken on July 3. For the 2010 *HST* data, no contemporaneous *XMM–Newton* observations are available, and individual *Swift* observations are too short to provide a meaningful constraint to the X-ray parameters. Therefore, we determined the *Swift* X-Ray Telescope (XRT) count rate at the time of the 2010 *HST* observations (*Swift* observation of 2010 September 23), and then stacked all *Swift* observations across the six observed outbursts that have an observed count rate within a factor of 2 of the count rate at the *HST* epoch.[1]

For the *HST* data, we downloaded the calibrated images (drizzled files) from NASA's Mikulski Archive for Space Telescopes. HLX-1 is a well-isolated source, with no risk of confusion with other nearby point-like sources. Therefore, we used aperture photometry to measure its brightness, with standard packages such as SAOImage DS9 version 7.4 and IRAF version 2.16. Particularly in the redder filters, proper background subtraction is crucial because of the strong unresolved emission from the old stellar population in ESO 243-49 and the gradient of such emission. For the source, we used a circular extraction region of radius 0.2 arcsec (Fig. 3). For

---

[1] We can build this average spectrum because we also verified that all *Swift* observations in that range of count rates (≈0.012–0.05 counts s⁻¹) have similar colours in a hardness–intensity diagram, consistent with the disc-dominated high/soft state; see also Yan et al. (2015).

Table 1. Summary of the *HST* observation log and results.

Date	Days after peak	Instrument	Filter	Central wavelength (Å)	Exposure time (s)	Brightness (Vegamag)	Brightness (ABmag)
2010-09-13	6	ACS SBC	*F140LP*	1528.0	2480	22.13 ± 0.15	24.30 ± 0.15
2010-09-23	16	WFC3 UVIS	*F300X*	2814.8	1710	22.60 ± 0.05	24.07 ± 0.05
			F390W	3922.9	712	23.83 ± 0.05	24.05 ± 0.05
			F555W	5308.2	742	24.04 ± 0.05	24.02 ± 0.05
			F775W	7647.6	740	23.71 ± 0.05	24.10 ± 0.05
		WFC3 IR	*F160W*	15 369.2	806	23.6 ± 0.3	24.9 ± 0.3
2012-11-19	72	ACS SBC	*F140LP*	1528.0	2428	22.53 ± 0.15	24.70 ± 0.15
		WFC3 UVIS	*F300X*	2814.8	1001	23.2 ± 0.1	24.7 ± 0.1
			F336W	3354.8	983	23.5 ± 0.1	24.7 ± 0.1
			F390W	3922.9	1068	24.33 ± 0.05	24.55 ± 0.05
			F555W	5308.2	1045	24.57 ± 0.05	24.55 ± 0.05
			F621M	6218.9	1065	24.40 ± 0.05	24.55 ± 0.05
			F775W	7647.6	1040	24.11 ± 0.05	24.50 ± 0.05
		WFC3 IR	*F105W*	10 551.0	1209	24.1 ± 0.2	24.7 ± 0.2
			F160W	15 369.2	1209	23.7 ± 0.3	25.0 ± 0.3
2013-07-05	300	ACS SBC	*F140LP*	1528.0	2428	23.83 ± 0.15	26.00 ± 0.15
		WFC3 UVIS	*F300X*	2814.8	1004	24.1 ± 0.1	25.6 ± 0.1
			F336W	3354.8	980	24.2 ± 0.1	25.4 ± 0.1
			F390W	3922.9	1074	25.2 ± 0.2	25.4 ± 0.1
			F555W	5308.2	1039	25.0 ± 0.1	25.0 ± 0.1
			F621M	6218.9	1077	24.85 ± 0.05	25.00 ± 0.15
			F775W	7647.6	1028	24.51 ± 0.15	24.90 ± 0.15
		WFC3 IR	*F105W*	10 551.0	1209	24.3 ± 0.2	24.9 ± 0.2
			F160W	15 369.2	1209	23.8 ± 0.3	25.1 ± 0.3

the background, we used an elliptical annulus oriented at a parallactic angle (north through east) of $75°$, that is approximately parallel to the isophotes of ESO 243-49 around the projected location of HLX-1. This was done to reduce the gradient of the unresolved emission in the background region. The semi-major axes of the outer background annulus were 1 and 0.45 arcsec; those of the inner (exclusion) annulus were 0.45 and 0.3 arcsec. For each filter and each epoch, we measured the background-subtracted count rate of HLX-1 within the 0.2 arcsec extraction region, and converted it to a 0.4 arcsec count rate. To do so, we selected isolated, brighter point-like sources in the same chip, and determined the ratio of the count rates from a 0.2 and 0.4 arcsec radius; as a safety check, we also compared our empirical values with the aperture correction values tabulated in the WFC3 and ACS online handbooks, and found them consistent. We then converted the 0.4 arcsec count rates to Vega and AB magnitudes, using the zero-point tables provided online by the Space Telescope Science Institute. Finally, we used the FTOOLS (Blackburn 1995) task *flx2xsp* to convert the observed *HST* flux densities into standard PHA files with their associated response files, which can be displayed and fitted in XSPEC (Arnaud 1996).

For *XMM–Newton*, we downloaded the data from NASA's High Energy Astrophysics Science Archive Research Center (HEASARC) archive: we used ObsID 0693060401 (PI: S. Farrell) from 2012 November 23, and ObsID 0693060301 (PI: S. Farrell) from 2013 July 4–5. We reprocessed the European Photon Imaging Camera (EPIC) MOS and pn observation data files with the Science Analysis System (SAS) version 14.0.0. We checked for exposure intervals with high particle background, and removed them from the analysis; the good time interval was 49 ks for the 2012 data set and 112 ks for the 2013 data set. We extracted the source photons from a circular region with a radius of 30 arcsec; the background photons were obtained from nearby regions located at similar distances from readout nodes, and avoiding chip gaps. We used the

sas task *xmmselect* to select single and double events (pattern 0–4 for pn and 0–12 for MOS1 and MOS2), and filtered them with the standard criteria FLAG $=0$ and #XMMEA_EP for the pn and #XMMEA_EM for the MOS. We built response and ancillary response files with the SAS tasks *rmfgen* and *arfgen*. Finally, to increase the signal-to-noise ratio, we combined the pn and MOS spectra with *epicspeccombine*, creating an average EPIC spectrum for each of the two epochs. We grouped the two combined spectra to a minimum of 20 counts per bin; coincidentally, this gives us ≈3 bins per spectral resolution element, keeping in mind that the spectral resolution of a combined EPIC spectrum is ≈100 eV at ≈0.3–2 keV. Finally, we fitted the 2012 and 2013 EPIC spectra with XSPEC version 12.8.2 (Arnaud 1996), together with the corresponding *HST* spectra.

For the *Swift*/XRT data, we used the online product generator (Evans et al. 2009) to extract a light curve, determine the count rate on 2010 September 23, and build a stacked spectrum with all the XRT observations between 2009 and 2015 with a count rate within a factor of 2 of the reference one. The stacked spectrum comprises 101 snapshot observations for a total exposure time of 66 ks. A similar stacking technique was previously used by other authors (e.g. Soria, Zampieri & Zane 2011; Yan et al. 2015) to model the characteristic high/soft, intermediate and low/hard state spectra. We verified that a stacked spectrum including only data from the 2010 outburst [similar to what was done by Farrell et al. (2012) for their broad-band modelling of X-ray and optical/UV data] produces similar results, but at lower signal-to-noise, which makes it harder to constrain the disc parameters.

2.3 Main results

The immediate result of our comparison between the three *HST* observations is the sharp decline in the bluest part of the optical/UV spectrum going from the high/soft to the low/hard X-ray state;
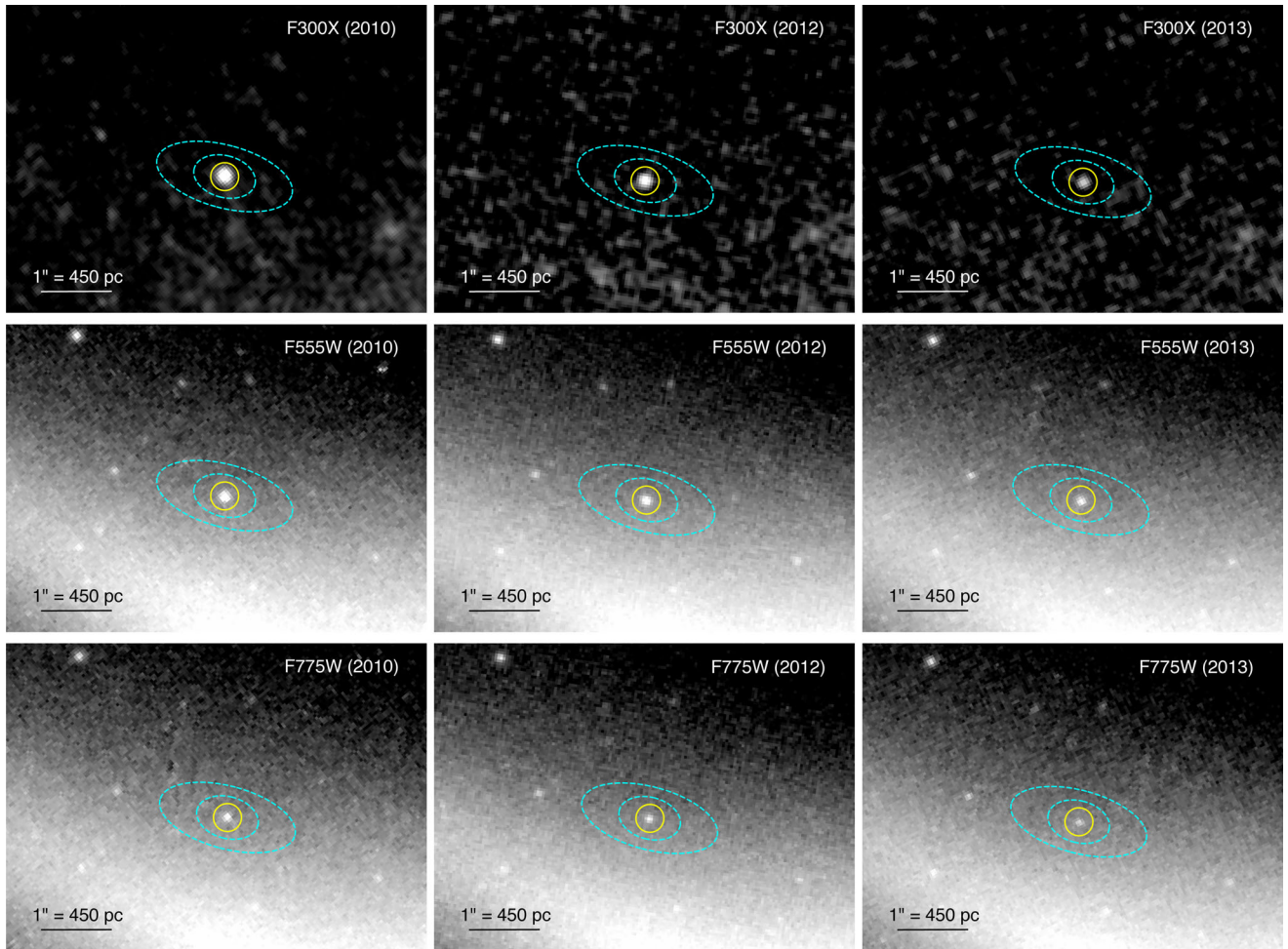
Figure 3. Zoomed-in view of HLX-1 from the *HST*/WFC3 images, at different epochs and for a selection of three different filters. North is up and east to the left. In each panel, the yellow circle (0.2 arcsec radius) is the source extraction region in our photometric analysis, while the background was extracted from the region between the two dashed ellipses. Top row: *F300X* filter; middle row: *F555W* filter; bottom row: *F775W* filter. In each row, we used the same grey-scale for the three epochs. The luminosity decline between the 2010 and 2013 data sets was 1.5 mag in the *F300X* filter, 1.0 mag in the *F555W* filter and 0.8 mag in the *F775W* filter.

instead, there is only a small flux decrease in the redder bands (Table 1 and Fig. 4). It was already known (Farrell et al. 2012, 2014; Soria et al. 2012a) that a single irradiated disc is not sufficient to reproduce the 2010 *HST* optical spectrum: either an additional near-IR component (possibly an old stellar population) or an additional near-UV component (possibly a young stellar population), or both, are needed. For each of the three *HST* epochs, we applied a code developed by Mucciarelli et al. (2007) and Patruno & Zampieri (2008), upgraded to calculate the magnitudes of an irradiated disc in the *HST* photometric bands (see also Mapelli et al. 2013a): like for the 2010 data, we verified that at least one additional component is required also for the 2012 and 2013 data. By comparing the three data sets, we have now proved the correlation between near-UV emission and the level of X-ray irradiation. Therefore, the near-UV emission in outburst cannot be dominated by a young stellar population, because of its variability; the near-UV luminosity in the faintest observed epoch (2013) sets the upper limit to the constant contribution of young stars. On the other hand, the near-IR component can be dominated by constant emission from an old stellar population.

Given the small number of optical/UV data points, and therefore the small number of free parameters we can introduce, we tried
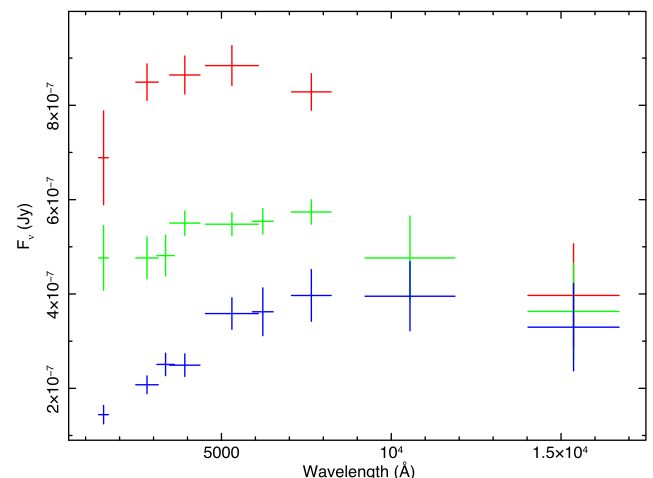
Figure 4. Red data points: optical flux densities in the 2010 *HST* data set (corresponding to the high/soft state); green data points: optical flux densities in the 2012 data set (intermediate state); blue data points: optical flux densities in the 2013 data set (low/hard state).

fitting the broad-band data with two simple models: one in which all of the near-UV emission comes from the irradiated disc at all epochs ('Model 1'), and one in which all of the near-UV emission in the faintest epoch (2013) comes from a young stellar population, and the additional irradiation component only appears in 2010 and 2012 ('Model 2'). Those are clearly extreme cases: in reality, the contribution from the young stellar population may be somewhere between the two cases.

Let us start with Model 1, which consists of an irradiated disc (*diskir* in XSPEC; Gierliński, Done & Page 2008, 2009) plus a constant, cool blackbody component (*bbodyrad*). The parameters of the blackbody component are determined from the 2013 observation, when it dominates the optical spectrum. These parameters are then kept fixed for our fits to the 2010 and 2012 *HST* data, dominated by the bluer component. We find (Fig. 5, Table 2) that we can reproduce the spectral energy distribution (SED) at all three epochs. The moderately high fit residuals in the 2010 data set ($\chi^2 \approx$ 1.25) are mostly due to the X-ray part of the spectrum (the stacked *Swift*/XRT data), and to a near-UV excess in the $F140LP$ filter. The latter is probably caused by the fact that this band was observed 10 d before the other *HST* bands, closer to outburst peak, and the near-UV is the most sensitive colour to the effect of X-ray irradiation. More detailed analyses and discussions of the 2010 *HST* and broad-band data have already been presented elsewhere (Farrell et al. 2012, 2014; Soria et al. 2012a; Mapelli et al. 2013a) and need not be repeated here. The new, interesting result of this work is that the irradiated disc plus blackbody model formally works also for the intermediate- and low-state observations. However, a very high reprocessing fraction $f_{out} \approx 4$ per cent is required in 2012 and 2013.

In simple terms, the high value of f_{out} in the 2012 and 2013 fits is because the blue flux (modelled with irradiation) decreases more slowly than the soft X-ray flux in the three *HST* epochs used for our modelling, from 2010 to 2012 and 2013. In 2010, the observed 0.3–10 keV flux was $f_X \approx 5.7 \times 10^{-13}$ erg cm^{-2} s^{-1}, and the flux at $\lambda > 912$ Å was $f_O \approx 2.4 \times 10^{-14}$ erg cm^{-2} s^{-1}, of which $f_R \approx 1.8 \times 10^{-15}$ erg cm^{-2} s^{-1} modelled as a constant red component. That gives a ratio $f_X/(f_O - f_R) \approx 26$ between the short- and long-wavelength emission of the accretion flow. In 2012, $f_X \approx 7.2 \times 10^{-14}$ erg cm^{-2} s^{-1} and $f_O \approx 1.4 \times 10^{-14}$ erg cm^{-2} s^{-1}, so that $f_X/(f_O - f_R) \approx 6$. In 2013, $f_X \approx 2.6 \times 10^{-14}$ erg cm^{-2} s^{-1} and $f_O \approx 6.2 \times 10^{-15}$ erg cm^{-2} s^{-1}, also for a ratio $f_X/(f_O - f_R) \approx 6$.

At first sight, such high levels of optical reprocessing appear difficult to explain. They are an order of magnitude higher than predicted by standard thin-disc models (Vrtilek et al. 1990; de Jong, van Paradijs & Augusteijn 1996; King, Kolb & Szuszkiewicz 1997; Dubus et al. 1999), supported by observations of sub-Eddington Galactic X-ray binaries (Hynes et al. 2002; Gierliński et al. 2009; Russell et al. 2014). In ultraluminous X-ray sources (ULXs), which in most cases are likely to be super-Eddington accretors, it is harder to distinguish between the emission from the donor star and from the irradiated disc (Tao et al. 2011, 2012; Grisé et al. 2012; Gladstone et al. 2013; Heida et al. 2014); therefore, it is also more difficult to determine the disc reprocessing fraction. In one ULX where all optical emission was proved to be from the irradiated disc (M83 ULX), a reprocessing factor of $\approx 5 \times 10^{-3}$ was inferred (Soria et al. 2012b); however, for other ULXs, broad-band emission models suggested reprocessing factors of a few 10^{-2} (Sutton, Done & Roberts 2014). The geometric solid angle subtended by the disc is insufficient to explain such reprocessing factors only from direct X-ray illumination; however, if there is a strong outflow launched from the inner part of the disc, it was suggested (Sutton, Done & Roberts 2014; Narayan, Sadowski & Soria 2017) that some of the X-ray photons

emitted along the polar funnel may be scattered isotropically and contribute to the illumination of the outer disc. In this paper, we argue that HLX-1 is a sub-Eddington source (IMBH accretor), so in that sense it would be more appropriate to compare its reprocessing fraction with those of Galactic X-ray binaries. On the other hand, we will also argue (Section 5.3) that it has a strong wind, which would be consistent with the photon scattering scenario proposed for ULXs and with a high reprocessing factor.

In fact, when we examine more carefully the physical meaning of f_{out} in 2012 and 2013, we propose other explanations for those high values. In 2012, optical and X-ray observations were not strictly simultaneous: the *XMM–Newton* observation happened 4 d after the *HST* observation. Those few days between the two observations are precisely the moment when HLX-1 started to switch from the high/soft to the low/hard state, with a drop in the *Swift*/XRT count rate by an order of magnitude (Fig. 2, bottom panel). Thus, when the *HST* measurements were taken, the X-ray flux was almost certainly a few times higher than what was measured with *XMM–Newton* a few days later. We fitted the *XMM–Newton* and *HST* data together without accounting for the decrease in the X-ray flux: this means that we are almost certainly overestimating by the same amount the true value of f_{out} needed to match the X-ray and UV portions of the SED. As for the high reprocessing fraction fitted to the 2013 data, we recall that our Model 1 represents the extreme case of no contribution from a young stellar population: in this sense, f_{out} here represents the hard upper limit to the reprocessing fraction in 2013. In the opposite case (Model 2), the same SED can be fitted with the other extreme case of $f_{out} \rightarrow 0$.

Let us consider now Model 2 (Table 3 and Fig. 6). We start from the 2013 data set, which gives us the constraint on the stellar contribution (no optical/UV disc emission). On the X-ray side, we replace the *diskir* model with a simple blackbody plus Comptonization model (*bbodyrad* + *comptt*), which does not extend into the UV. On the optical/UV side, we fit the 2013 spectrum only with two blackbody components, one bluer and one redder, with no additional contribution from a disc. Having determined the old and young stellar contributions from the 2013 data (Table 3), we impose that the same two components are also present in the 2010 and 2012 spectra with the same (fixed) temperature and normalization, in addition to an irradiated disc component.

In summary, we find that Models 1 and 2 are statistically equivalent in all three epochs (compare Tables 2 and 3). We cannot tell the difference between the scenarios of near-UV emission from the disc only, or from a young stellar population plus an irradiated disc. However, we can use the models to calculate the age and mass of the old stellar populations, and to put useful upper limits to the young stellar population. In Model 1, with only a red component, the best-fitting blackbody temperature corresponds to a dereddened $V = 25.56 \pm 0.10$ mag in the Vega system, with $V - I = 1.03 \pm 0.15$ mag, $B - V = 0.82 \pm 0.15$ mag. At a distance modulus of 34.8 mag (92 Mpc), the absolute brightness is $M_V \approx -9.2$ mag. We ran simulations of star cluster evolution with Starburst99 version 7.0.1 (Leitherer et al. 1999, 2014), for instantaneous star formation and metallicity $Z = 0.008$. We found that those optical colours and luminosities are consistent either with an intermediate-age star cluster with mass $M_* \approx 2 \times 10^5$ M$_\odot$ and age of ≈ 800–900 Myr, or with an old star cluster, in particular one with a mass $M_* \approx 3 \times 10^6$ M$_\odot$ and age of ≈ 6–8 Gyr (Fig. 7). We repeated the same analysis for Model 2, with two optical blackbody components (Table 3). The colder component has a dereddened $V = 25.41 \pm 0.10$ mag, $V - I = 0.93 \pm 0.15$ mag, $B - V = 0.76 \pm 0.15$ mag, similar to the red component in the first model. The hotter
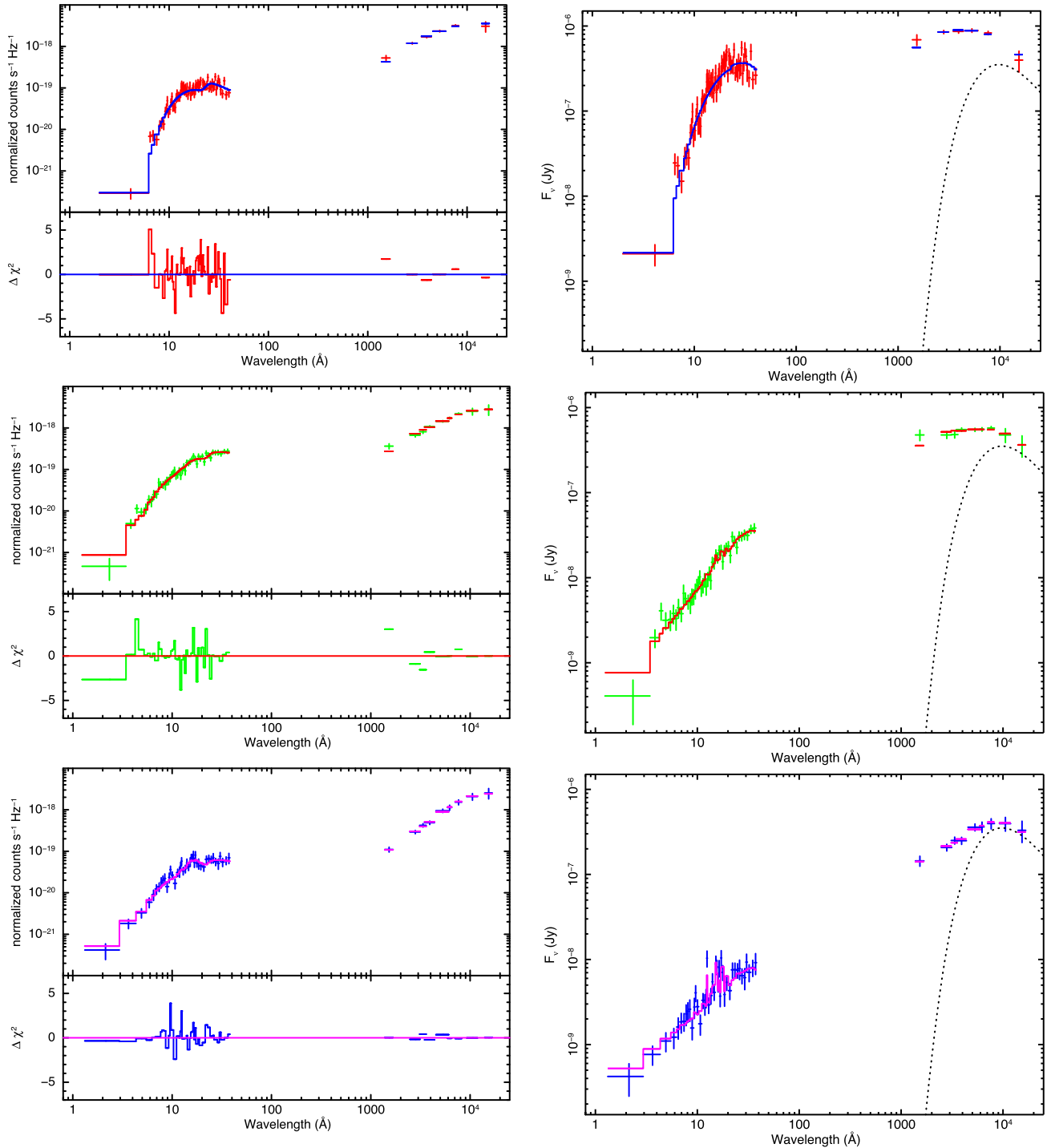
Figure 5. Top row, left-hand panel: SED and fit residuals for the broad-band spectrum of HLX-1 in the high/soft state (2010 *HST* data plus stacked *Swift* spectrum), fitted with the model summarized in Table 2 (Model 1). Top row, right-hand panel: unfolded spectrum of the high/soft state; the dotted line represents the constant blackbody component (which we attribute to an old stellar population) in our model. Middle row, left-hand panel: fitted spectrum and residuals in the intermediate state (2012 *HST* and *XMM–Newton* data). Middle row, right-hand panel: unfolded spectrum in the intermediate state, with the constant blackbody component marked by a dotted line. Bottom row, left-hand panel: fitted spectrum and residuals in the low/hard state (2013 *HST* and *XMM–Newton* data). Bottom row, right-hand panel: unfolded spectrum in the low/hard state, with the blackbody component marked by a dotted line.

component has $V = 26.23 \pm 0.10$ mag, $V - I = -0.28 \pm 0.15$ mag, $B - V = -0.08 \pm 0.15$ mag. This is roughly consistent with the colours of a very young star cluster (age $\lesssim 3$ Myr), with a mass $\lesssim 10^4\,\mathrm{M_\odot}$, which can be taken as the firm upper limit to the young

stellar component associated with HLX-1. More detailed spectral modelling, with proper SEDs for stellar populations of various ages and metallicities, in place of simple blackbody components, is left to follow-up work (Maraston, private communication).

Table 2. Spectral parameters of our X-ray/optical spectral fitting for the three epochs of *HST* observations. The model ('Model 1') is *redden*$_{los}$ × *redden* × *TBabs*$_{los}$ × *TBabs* × (*diskir* + *bbodyrad*) + *TBabs*$_{los}$ × *mekal* (the last term accounts for the contamination of thermal emission from ESO 243-49). Errors are 90 per cent confidence limits for one interesting parameter.

Component	Parameter	Epoch 2010 Sept.	2012 Nov.	2013 July
redden$_{los}$	$E(B-V)_{los}$ (mag)	[0.013]	[0.013]	[0.013]
redden	$E(B-V)$ (mag)	<0.12	<0.12	<0.11
TBabs$_{los}$	$N_{H, los}$ (10^{20} cm^{-2})	[2.0]	[2.0]	[2.0]
TBabs	N_H (10^{20} cm^{-2})	<1.3	<1.4	<2.0
diskir	kT_{in} (keV)	$0.22^{+0.01}_{-0.01}$	$0.083^{+0.037}_{-0.040}$	<0.073
	Γ	$1.8^{+2.1}_{-0.6}$	$2.43^{+0.15}_{-0.15}$	$2.04^{+0.26}_{-0.20}$
	kT_e (keV)	[100]	[100]	[100]
	L_c/L_d	$0.12^{+1.35}_{-0.09}$	$2.1^{+*}_{-0.9}$	$16.8^{+*}_{-15.4}$
	f_{in}	[0.1]	[0.1]	[0.1]
	r_{irr}	[1.2]	[1.2]	[1.2]
	f_{out} (10^{-3})	$6.6^{+1.5}_{-3.5}$	43^{+*}_{-16}	45^{+23}_{-15}
	$\log(R_{out})$	$3.68^{+0.05}_{-0.06}$	$3.27^{+0.30}_{-0.24}$	<3.16
	K^a	$17.6^{+12.2}_{-4.4}$	$39.5^{+139}_{-28.5}$	>3.0
bbodyrad	T_{bb} (K)	[5270]	[5270]	5270^{+300}_{-400}
	N_{bb} (10^9)^b	[3.9]	[3.9]	$3.9^{+0.7}_{-0.9}$
mekal	kT_{mk} (keV)	[0.45]	[0.45]	$0.45^{+0.14}_{-0.13}$
	N_{mk} (10^{-6})	[1.1]	[1.1]	$1.1^{+0.7}_{-0.5}$
	f_X (10^{-14} erg cm^{-2} s^{-1})^c	57^{+3}_{-3}	$7.2^{+0.4}_{-0.2}$	$2.6^{+0.2}_{-0.2}$
	$L_X\cos\theta$ (10^{40} erg s^{-1})^d	$33.1^{+1.8}_{-1.9}$	$4.1^{+0.3}_{-0.2}$	$2.8^{+0.4}_{-0.2}$
	f_O (10^{-14} erg cm^{-2} s^{-1})^e	$2.4^{+0.1}_{-0.1}$	$1.4^{+0.1}_{-0.1}$	$0.60^{+0.02}_{-0.02}$
	f_R (10^{-14} erg cm^{-2} s^{-1})^f	[0.18]	[0.18]	$0.18^{+0.04}_{-0.05}$
	$R_{in}\sqrt{\cos\theta}$ (10^8 cm)	46^{+14}_{-6}	68^{+61}_{-32}	>20
	χ^2_ν	1.29 (91.3/71)	0.88 (64.3/73)	0.75 (61.5/82)

$^a K \equiv (r_{in}/\text{km})^2 (10\,\text{kpc}/d)^2 \cos\theta$.
$^b N_{bb} \equiv (R_{bb}/\text{km})^2 (10\,\text{kpc}/d)^2$.
^{c}Observed flux in the 0.3–10 keV band (not including the *mekal* component).
^{d}Unabsorbed luminosity in the 0.3–10 keV band (not including the *mekal* component); $L_X \equiv (2\pi d^2/\cos\theta) f_X$ for the 2010 (high) and 2012 (intermediate) state, and $L_X \equiv 4\pi d^2 f_X$ for the 2013 (low) state.
^{e}Total observed flux at $\lambda > 912$ Å.
^{f}Observed flux that is attributed to a constant red component.

The 2013 X-ray spectral fit is statistically improved (with *F*-test significance >99.9 per cent) by the addition of a thermal plasma component (*mekal* model in XSPEC), with solar abundance and fixed redshift $z = 0.0224$. We determined the temperature and normalization of the thermal plasma emission using the same strategy that we applied to the optical blackbody components: namely, we left those two *mekal* parameters free to vary in the 2013 spectrum, determined their best-fitting values, and then kept them frozen in the 2010 and 2012 spectra, assuming that the thermal plasma component does not vary on short time-scales. (In the 2010 and 2012 X-ray spectra, the additional thermal plasma component also improves the fit but with <90 per cent significance, because of the comparatively stronger disc emission.) We found a best-fitting *mekal* temperature of ≈(0.5 ± 0.1) keV, and a de-absorbed luminosity of ≈(3.3 ± 1.3) × 10^{39} erg s^{-1}, almost identical in Models 1 and 2. This is also the same thermal plasma temperature and luminosity that was found by Servillat et al. (2011) in an earlier *XMM–Newton* spectrum from

2010 May 14, also in the low/hard state (in between the 2009 and 2010 outbursts). Servillat et al. (2011) used the higher spatial resolution of *Chandra*/ACIS-S to show (see their sections 3.2–3.3) that the soft thermal component is likely to be diffuse emission from the bulge of ESO 243-49 rather than from HLX-1. Such extended component cannot be resolved in *XMM–Newton* (the 30 arcsec source extraction region for HLX-1 includes also the nuclear region and most of the galaxy). Thus, the thermal plasma emission seen in the *XMM–Newton* spectra of HLX-1 may have a different physical interpretation than the thermal plasma emission seen in several ULXs (Middleton et al. 2015; Sutton, Roberts & Middleton 2015; Pinto, Middleton & Fabian 2016; Urquhart & Soria 2016). In the latter group of sources, the line residuals appear to come from massive outflows, directly associated with the accreting compact objects; they are interpreted as evidence that those sources are stellar-mass BHs or neutron stars accreting much above their Eddington limit. The lack of intrinsic X-ray thermal plasma features in the HLX-1

Table 3. Spectral parameters of our X-ray/optical spectral fitting for the three epochs of *HST* observations ('Model 2'). For 2010 and 2012, the model is $redden_{los} \times redden \times TBabs_{los} \times TBabs \times (diskir + bbodyrad + bbodyrad) + TBabs_{los} \times mekal$ (the last term accounts for the contamination of thermal emission from ESO 243-49). For 2013, the model is $redden_{los} \times redden \times TBabs_{los} \times TBabs \times [(bbodyrad + comptt) + bbodyrad + bbodyrad] + TBabs_{los} \times mekal$. Errors are 90 per cent confidence limits for one interesting parameter.

Component	Parameter	Epoch		
		2010 Sept.	2012 Nov.	2013 July
$redden_{los}$	$E(B-V)_{los}$ (mag)	[0.013]	[0.013]	[0.013]
$redden$	$E(B-V)$ (mag)	<0.10	<0.15	[0.0]
$TBabs_{los}$	$N_{H, los}$ (10^{20} cm^{-2})	[2.0]	[2.0]	[2.0]
$TBabs$	N_H (10^{20} cm^{-2})	$2.0^{+2.8}_{-2.0}$	<1.4	<28
$bbodyrad_X$	kT_{bb} (keV)	–	–	$0.058^{+0.059}_{-0.058}$
	N_{bb} [a]	–	–	$37.7^{+*}_{-37.7}$
$comptt$	kT_0 (keV)	–	–	$[0.058^{+0.059}_{-0.058}]$[b]
	kT_e (keV)	–	–	[100]
	τ	–	–	$0.19^{+0.15}_{-0.07}$
	N_c (10^{-7})	–	–	$3.6^{+*}_{-1.9}$
$diskir$	kT_{in} (keV)	$0.21^{+0.02}_{-0.03}$	$0.086^{+0.03}_{-0.04}$	–
	Γ	$2.1^{+*}_{-1.0}$	$2.45^{+0.17}_{-0.21}$	–
	kT_e (keV)	[100]	[100]	–
	L_c/L_d	$0.066^{+9.5}_{-0.041}$	$2.0^{+*}_{-0.6}$	–
	f_{in}	[0.1]	[0.1]	–
	r_{irr}	[1.2]	[1.2]	–
	f_{out} (10^{-3})	$3.6^{+7.4}_{-3.1}$	27^{+*}_{-12}	–
	$\log(R_{out})$	$3.57^{+0.13}_{-0.18}$	$3.16^{+0.30}_{-*}$	–
	K[c]	$27.5^{+35.4}_{-11.1}$	$36.5^{+89}_{-26.5}$	–
$bbodyrad_B$	T_{bb} (K)	[21 170]	[21 170]	$21\,170^{+3760}_{-2890}$
	N_{bb} (10^9)[a]	[3.6]	[3.6]	$3.6^{+2.3}_{-1.4}$
$bbodyrad_R$	T_{bb} (K)	[5550]	[5550]	5550^{+250}_{-290}
	N_{bb} (10^9)[a]	[3.4]	[3.4]	$3.4^{+3.0}_{-1.7}$
$mekal$	kT_{mk} (keV)	[0.44]	[0.44]	$0.44^{+0.14}_{-0.13}$
	N_{mk} (10^{-6})	[1.1]	[1.1]	$1.1^{+0.7}_{-0.5}$
	f_X (10^{-14} erg cm^{-2} s^{-1})[d]	57^{+2}_{-2}	$7.2^{+0.4}_{-0.2}$	$2.6^{+0.2}_{-0.2}$
	$L_X \cos\theta$ (10^{40} erg s^{-1})[e]	$38.1^{+6.0}_{-4.9}$	$4.1^{+0.3}_{-0.2}$	$2.8^{+0.4}_{-0.2}$
	f_O (10^{-14} erg cm^{-2} s^{-1})[f]	$1.9^{+0.1}_{-0.1}$	$1.3^{+0.1}_{-0.1}$	$0.56^{+0.04}_{-0.04}$
	f_B (10^{-14} erg cm^{-2} s^{-1})[g]	[0.37]	[0.37]	$0.37^{+0.03}_{-0.01}$
	f_R (10^{-14} erg cm^{-2} s^{-1})[h]	[0.19]	[0.19]	$0.19^{+0.02}_{-0.04}$
	$R_{in}\sqrt{\cos\theta}$ (10^8 cm)	57^{+30}_{-13}	66^{+57}_{-31}	–
	χ^2_ν	1.25 (88.9/71)	0.89 (64.8/73)	0.73 (61.7/85)

[a] $N_{bb} \equiv (R_{bb}/km)^2 (10\,kpc/d)^2$.
[b] Seed temperature of the *comptt* model locked to the blackbody temperature.
[c] $K \equiv (r_{in}/km)^2 (10\,kpc/d)^2 \cos\theta$.
[d] Observed flux in the 0.3–10 keV band (not including the *mekal* component).
[e] Unabsorbed luminosity in the 0.3–10 keV band (not including the *mekal* component); $L_X \equiv (2\pi d^2/\cos\theta) f_X$ for the 2010 (high) and 2012 (intermediate) states, and $L_X \equiv 4\pi d^2 f_X$ for the 2013 (low) state.
[f] Total observed flux at $\lambda > 912$ Å.
[g] Observed flux at $\lambda > 912$ Å, attributed to a constant blue component.
[h] Observed flux that is attributed to a constant red component.

spectra, on the other hand, is consistent with the interpretation of this source as an IMBH accreting at an Eddington rate $\lesssim 1$. For these reasons, we did not include the flux and luminosity of the thermal plasma component in the values of f_X and L_X reported in Tables 2 and 3.

3 WHAT IS THE MASS OF THE BH?

The normalization of the *diskir* model (i.e. the fitted inner radius of the disc) in the high/soft and intermediate state (Tables 2 and 3) is consistent between Models 1 and 2. By taking a weighted average
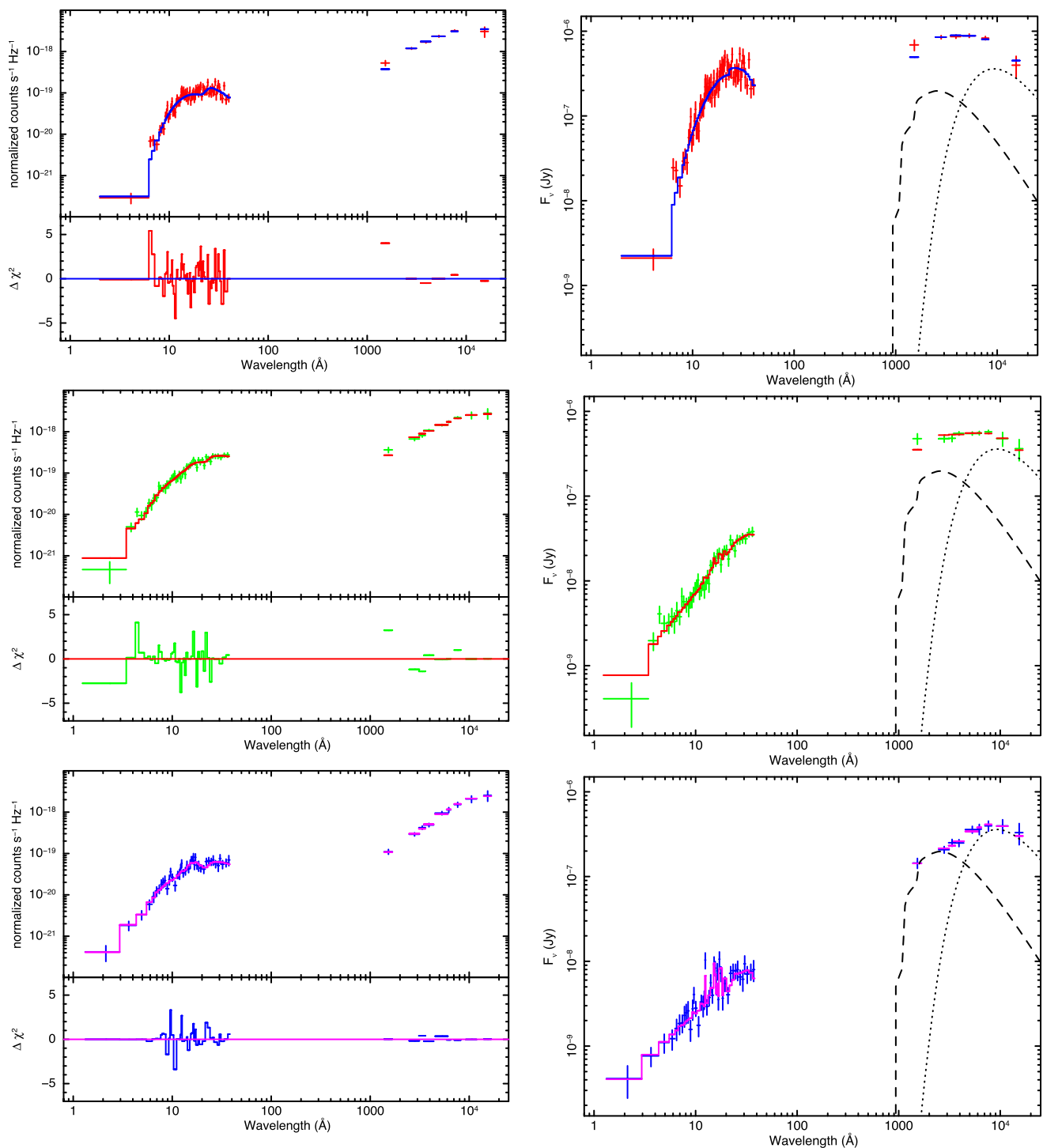
Figure 6. Top row, left-hand panel: SED and fit residuals for the broad-band spectrum of HLX-1 in the high/soft state (2010 *HST* data plus stacked *Swift* spectrum), fitted with the model summarized in Table 3 (Model 2). Top row, right-hand panel: unfolded spectrum of the high/soft state; the dotted line is the redder blackbody component (which we attribute to an old stellar population), and the dashed line is the bluer blackbody component (which we associate with a younger stellar population) in our model. Middle row, left-hand panel: fitted spectrum and residuals in the intermediate state (2012 *HST* and *XMM–Newton* data). Middle row, right-hand panel: unfolded spectrum in the intermediate state, with the constant red and blue blackbody components marked by a dotted and a dashed line, respectively. Bottom row, left-hand panel: fitted spectrum and residuals in the low/hard state (2013 *HST* and *XMM–Newton* data). Bottom row, right-hand panel: unfolded spectrum in the low/hard state, with the red and blue blackbody components marked by a dotted and a dashed line, respectively.

of the four best-fitting values from the high and intermediate state (two from Model 1 and two from Model 2), we obtain

$$R_{\rm in}\sqrt{\cos\theta} \approx 1.19\, r_{\rm in}\sqrt{\cos\theta} \approx \left(49.3^{+12.4}_{-5.6}\right) \times 10^3 \ {\rm km}, \quad (1)$$

where the factor 1.19 takes into account the hardening factor and the inner-boundary condition, as discussed in Kubota et al. (1998). (Notice that the four values used for this average are all consistent with each other within their errors.) Our best-fitting inner-disc radius
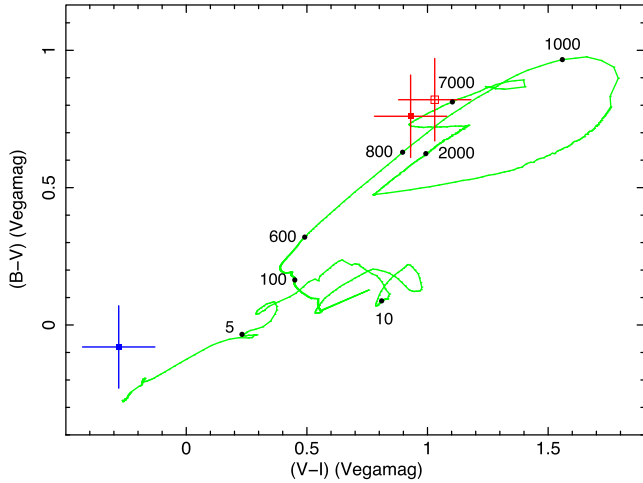
Figure 7. Open red square: dereddened optical colours (Vegamag system) of the cooler blackbody component ($T \approx 5300$ K) in the optical spectrum of HLX-1, for Model 1. Filled red square: dereddened colours of the cooler component ($T \approx 5500$ K) in Model 2. Filled blue square: dereddened colours of the hotter blackbody component ($T \approx 21\,000$ K) in Model 2. Green curve: predicted colours of a single-population star cluster as a function of age. A few characteristic ages in Myr have been labelled along the curve.

Figure 8. Evolution of HLX-1 on the hardness–intensity plane, based on the observed EPIC-pn count rates in various observations. The hardness ratio (X axis) is defined as the ratio between the pn count rates in the 1–10 and 0.3–1 keV bands. The intensity (Y axis) is the pn count rate in the 0.3–10 keV band. Red data points correspond to the *XMM–Newton* observations analysed in this work; black data points are from Servillat et al. (2011). Observation dates are labelled.
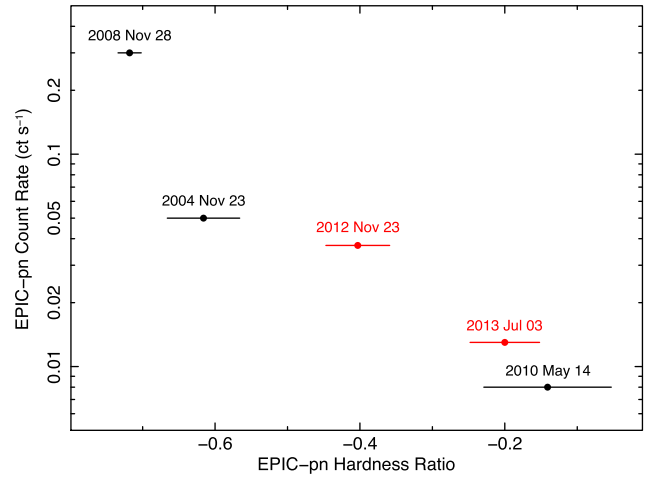
is also consistent with those previously published in the literature (Farrell et al. 2009b, 2012, 2014; Soria et al. 2011, 2012a; Godet et al. 2012). Instead, in the low/hard state, the size of the thermal seed component (disc blackbody in the *diskir* model and blackbody in the *comptt* model) cannot be constrained: the data are also consistent with seed temperatures $\lesssim 50$ eV (a range in which they can no longer be meaningfully constrained with the EPIC detectors), and a correspondingly larger normalization. The *diskir* model does suggest that $R_{\rm out}/R_{\rm in} \lesssim 1400$ in the low/hard state (Table 2), a few times less than in the high state (when $R_{\rm out}/R_{\rm in} \approx 4000\text{–}5000$); if we assume that the outer-disc radius remains approximately constant (as determined in Section 4.2), it means that the inner radius is moving further out (truncated disc), to a value $R_{\rm in} \gtrsim 2 \times 10^5$ km, consistent with the canonical evolution of an accretion disc in BH transients at the end of an outburst.

Henceforth, we will use only the high-state and intermediate-state spectra for an estimate of the inner-disc radius and BH mass. The fact that in several disc-dominated X-ray spectra, measured with different instruments over different outbursts, the inner-disc radius is consistently found to be $R_{\rm in} \sqrt{\cos\theta} \approx 50\,000\text{–}100\,000$ km (see also table 3 in Farrell et al. 2014) suggests that this parameter is physically meaningful, representing the innermost stable circular orbit $R_{\rm isco}$. We introduce a parameter $\alpha_{\rm s}$ to express the innermost stable orbit as a function of the gravitational radius, such that $R_{\rm in} = R_{\rm isco} \equiv \alpha_{\rm s} GM/c^2$, where $1 < \alpha_{\rm s} \leq 6$, depending on the BH spin. In the framework of the standard disc model, the BH mass is then

$$M \approx \frac{(3.3^{+0.9}_{-0.4})}{\alpha_{\rm s} \sqrt{\cos\theta}} \times 10^4 \, {\rm M}_\odot. \qquad (2)$$

If we assume that the peak of each outburst corresponds to the Eddington luminosity (in the X-ray band), we obtain $M \approx 1 \times 10^4 \, {\rm M}_\odot$ and $\alpha_{\rm s} \sqrt{\cos\theta} \approx 3.3$. However, there is no compelling reason for assuming Eddington-limited outbursts: many Galactic X-ray transients peak at only a fraction of Eddington (Fender et al. 2004; Remillard & McClintock 2006).

Fortunately, the *XMM–Newton* spectrum from 2012 November 23 provides new information on a particularly interesting stage of

the outburst cycle, and an additional independent constraint to the BH mass. In the model-independent hardness–intensity diagram, based on the observed EPIC-pn count rates, we note (Fig. 8) that the position of the source appears to fall in between the high/soft and the low/hard state. Using Galactic X-ray binary terminology, we could say that the system was on the lower/descending branch of the so-called *Q* diagram, which is often used to describe phenomenologically the evolution of stellar-mass BH transients (Fender et al. 2004). In fact, a full '*Q*' cycle has never been observed for HLX-1, perhaps because the outburst rise in the hard state and the transition to the soft state occur very quickly; based on *Swift* data, the hardness–intensity diagram for HLX-1 shows two clear states but little evidence of the track between the two (Yan et al. 2015). Regardless of the actual shape of the outburst cycle, the 2012 data suggest that HLX-1 was in the middle of the (fairly rapid) transition from the soft to the hard state. This scenario is confirmed by the sharp decline in the *Swift*/XRT count rate that occurs right at the time of the 2012 observation (Fig. 2, bottom panel), over a time-scale of less than a week. Our spectral modelling shows (Tables 2 and 3) that disc and Comptonized (power-law) components contribute at comparable levels; the power-law photon index is still relatively soft ($\Gamma \approx 2.2$), while the peak disc temperature $kT_{\rm in} \approx 120$ eV is a factor of 2 below the temperature at outburst peak.

Empirical evidence from Galactic X-ray transients shows that the soft-to-hard state transition at the end of an outburst occurs at a characteristic luminosity $L \approx L_{\rm X} \approx 0.01\text{–}0.03 \, L_{\rm Edd}$ (Maccarone 2003; Kalemci et al. 2013). We determined a deabsorbed luminosity $L_{\rm X} = (4.1^{+0.3}_{-0.2} \times 10^{40})/\cos\theta$ erg s^{-1} for the 2012 *XMM–Newton* data, assuming a disc-like emission geometry. Taking $L_{\rm Edd} \approx 1.3 \times 10^{38} (M/{\rm M}_\odot)$ erg s^{-1}, we obtain

$$M \approx \frac{1.6^{+1.7}_{-0.6}}{\cos\theta} \, 10^4 \, {\rm M}_\odot. \qquad (3)$$

Combining equations (2) and (3), we derive

$$\alpha_{\rm s} \approx \left(2.1^{+1.3}_{-1.1}\right) \sqrt{\cos\theta}. \qquad (4)$$

Since $\cos\theta \leq 1$, $R_{\rm isco} \lesssim 3.4 GM/c^2$, which implies that the BH spin parameter $a/M \gtrsim 0.7$. We do not have any direct measurements of

cos θ; however, the low absorbing column density required by the X-ray spectral fits suggests that HLX-1 is more likely not seen at very high inclination. This is also consistent with the viewing angle $\theta \approx 30°$ proposed by Cseh et al. (2015) to model the Doppler boosting of the radio jet in the low/hard state. The central value of our estimate (corresponding to a soft-to-hard transition luminosity of $0.02 L_{\rm Edd}$) is $\alpha_s \approx 2.1$ for $\theta \approx 0°$, $\alpha_s \approx 2.0$ for $\theta \approx 30°$, $\alpha_s \approx 1.8$ for $\theta \approx 45°$. This implies a spin parameter $a/M \approx 0.9$, almost independent of θ, for $\theta \lesssim 45°$.

In conclusion, from the transition luminosity and the fitted inner-disc radius, and for moderately face-on viewing angles, we estimate a BH mass $M \approx (2 \pm 1) \times 10^4 \, {\rm M}_\odot$, a BH spin parameter $\gtrsim 0.7$ for any viewing angle, and ≈ 0.9 for face-on angles, and a peak outburst luminosity $L_{\rm X} \approx (0.3 \pm 0.15) L_{\rm Edd}$. Our best-fitting values of mass and spin are very similar to those inferred by Davis et al. (2011, see in particular their fig. 5) from *Swift* data, in the case of $\theta \approx 0$. Our best-fitting BH mass is also similar to the value found by Godet et al. (2012), although the latter result was based on slim-disc models, which may not be relevant if the peak luminosity is always sub-Eddington. Note that our value of the peak outburst luminosity is about half the value usually reported in the literature (e.g. Farrell et al. 2009b, 2012; Yan et al. 2015), because we have defined luminosities as $(2\pi d^2 / \cos\theta)$ times the flux (as more suitable to disc-dominated emission) rather than $4\pi d^2$ times the flux.

If we assume instead a perfectly isotropic emission during the 2012 intermediate state, the luminosity becomes $L_{\rm X} = (8.2^{+0.6}_{-0.4} \times 10^{40})$ erg s^{-1} ≈ 0.01–$0.03 \, L_{\rm Edd}$. Repeating the same derivation, we obtain $M \approx (3.3^{+3.4}_{-1.1}) \times 10^4 \, {\rm M}_\odot$, and $\alpha_s \sqrt{\cos\theta} = 1.1^{+0.7}_{-1.1}$. For a moderately face-on view, this implies an even higher BH spin, close to an extreme Kerr BH. The peak outburst luminosity would be $L_{\rm X} \approx (0.15 \pm 0.08)/(\cos\theta \, L_{\rm Edd})$.

4 HOW LARGE IS THE DISC?

Following Soria (2013), we estimate the outer radius $R_{\rm out}$ of the accretion disc in two independent ways. The first method is to assume that the X-ray luminosity during the initial phase of outburst decline has an exponential-decay time-scale of the order of the viscous time-scale at the outer edge of the disc. This can be understood in the framework of thin accretion disc models (e.g. Frank, King & Raine 2002); it also has an empirical analogy with the temporal brightness variations of Galactic X-ray binaries during their outbursts (King & Ritter 1998). The second method assumes that the optical emission comes mostly from the irradiated disc (as discussed in Section 2.3): the characteristic size of the thermal emitter is derived from the observed optical luminosity and temperature.

4.1 Disc size from X-ray outburst properties

During the 2009, 2010 and 2011 outbursts, the X-ray emission shows characteristic exponential-decay time-scales $\tau \approx (3$–$6) \times 10^6$ s (Soria 2013). For the 2012, 2013 and 2015 outbursts, the *e*-folding decay time-scales are shorter, $\tau \approx 2 \times 10^6$ s (Yan et al. 2015), although this value is possibly affected by the earlier transition from the exponential to the linear decay phase (fig. 6 in Yan et al. 2015). Such differences between outbursts are not crucial for our attempt to provide an order-of-magnitude estimate of the disc size. Exponential-decay time-scales of a few weeks are near the upper limit but still within the range of those observed in Galactic X-ray binary transients (Chen, Shrader & Livio 1997; Yan & Yu 2015), despite the much higher BH mass proposed by the IMBH scenario.

During the exponential decline of an outburst, when the rate of mass depletion in the disc (via accretion and/or outflows) is much higher than any ongoing mass transfer from the companion star, the decay time-scale is related to the outer-disc radius by the relation (Frank et al. 2002):

$$\tau \approx R_{\rm out}^2/(3\nu), \tag{5}$$

where ν is the kinematic viscosity. In the Shakura–Sunyaev model (Shakura & Sunyaev 1973), $\nu = \alpha c_s H$, where $\alpha \sim 0.1$–0.5 is a scaling parameter (not to be confused with the BH spin parameter used in Section 3), c_s is the mid-plane sound speed in the outer disc and H is the disc scaleheight. In the simplest empirical approximation, we can take $\alpha(H/R) \sim 0.01$ (Shahbaz, Charkles & King 1998). Then, $R_{\rm out} \sim 0.03 c_s \tau$. For HLX-1, we expect characteristic mid-plane temperatures $T \sim$ a few 10^5 K in the outer disc (Frank et al. 2002); hence, $c_s \sim 40$–60 km s^{-1} and $R_{\rm out} \sim 10^{12}$ cm. Using a more accurate expression of ν from the Shakura–Sunyaev disc solutions with Kramer's opacity (Shakura & Sunyaev 1973; Frank et al. 2002), for the observed X-ray properties of HLX-1, we re-obtain a characteristic disc radius $\lesssim 10^{12}$ cm (equation 10 in Soria 2013) for the earlier outbursts. For the time-scales measured in the most recent outbursts, a more likely estimate of the characteristic radius is $R_{\rm out} \sim$ a few 10^{11} cm.

When the disc is completely ionized (a condition expected to be easily satisfied in HLX-1; Lasota et al. 2011), the mass content in the disc declines exponentially on the viscous time-scale (King & Ritter 1998) after the peak of the outburst. This leads to a relation (Shahbaz et al. 1998) between outer-disc radius and peak luminosity $L_{\rm peak}$:

$$R_{\rm out} \approx 1.0 \times 10^{12} \left(\frac{\eta}{0.1}\right)^{-1/3} \left(\frac{L_{\rm peak}}{10^{42} \, {\rm erg \, s^{-1}}}\right)^{1/3} \left(\frac{\tau}{10^6 \, {\rm s}}\right)^{1/3} \, {\rm cm}, \tag{6}$$

where $\eta \equiv L/(\dot{m}c^2)$ is the radiative efficiency. Again, for the observed decline time-scales and peak luminosity, and efficiency $\eta \approx 0.3$ (suitable to a fast-spinning BH), we obtain that $R_{\rm out} \approx 10^{12}$ cm, consistent with our previous estimate.

Another (not entirely independent) estimate of disc size is based on the total fluence or energy released during an outburst. For HLX-1, the energy emitted as X-rays (which is a sufficiently good approximation to the total energy, for our order-of-magnitude estimate) declined from $\approx 10^{49}$ to $\approx 4 \times 10^{48}$ erg over the six recorded outbursts (table 3 in Yan et al. 2015), assuming isotropic emission, or a factor of 2 lower if we are looking at a face-on disc geometry. For a standard BH accretion efficiency $\eta \approx 0.1$, this energy corresponds to accreted masses between $\approx 10^{29}$ and $\approx 4 \times 10^{28}$ g, in the earliest and latest outbursts, respectively. These values may be reduced by up to a factor of 2 in the case of a face-one disc view, and another factor of 3 for a fast-spinning BH with $a/M \approx 0.9$. Considering the uncertainties, we can say that $10^{29} (0.1/\eta)$ g is a conservative upper limit to the mass accreted in each outburst. Surface density profiles $\Sigma(R)$ for irradiated discs around a $10 \, {\rm M}_\odot$ BH, for various accretion rates, were calculated by Dubus et al. (1999). The main effect of irradiation is to keep the outer disc in the hot state; in that regime, the surface density is well approximated by the Shakura–Sunyaev solution

$$\Sigma \approx 5.2 \times 10^3 \, \alpha^{-4/5} \, \dot{M}_{21}^{7/10} \, M_4^{1/4} \, R_{12}^{-3/4} \, {\rm g \, cm^{-2}} \tag{7}$$

(Shakura & Sunyaev 1973; Frank et al. 2002), where M_4 is the BH mass in units of $10^4 \, {\rm M}_\odot$ and $\dot{M}_{21}$ the accretion rate in units of 10^{21} g s^{-1} (suitable order of magnitude for the long-term-average

accretion rate in HLX-1). The total mass M_{tot} in the disc up to a radius R is given by

$$M_{tot}(R) \approx 2\pi \int_0^R \Sigma \, R \, dR$$
$$\approx 2.6 \times 10^{28} \, \alpha^{-4/5} \, \dot{M}_{21}^{7/10} \, M_4^{1/4} \, R_{12}^{5/4} \text{ g.} \tag{8}$$

Since the accreted mass during an outburst is $\lesssim 10^{29} (0.1/\eta)$ g, and taking $\alpha \lesssim 0.3$, $M_4 \approx 2$, from equation (8) we conclude that a typical outburst can empty a disc (or a substantial fraction of the disc) of radius $R \lesssim 10^{12}$ cm. If we also account for the factor-of-2 reduction in the mass accreted in each outburst (in the case of a face-on disc view), the disc size (or at least the portion of the disc) that can be emptied in each outburst is only $R \lesssim 5 \times 10^{11}$ cm.

A radius $\sim$ a few 10^{11}–10^{12} cm is within the range of disc sizes in stellar-mass Galactic BH X-ray binaries (fig. 1 in Remillard & McClintock 2006); for example, it would be smaller than the disc in GRS 1915+105 ($R_{out} \approx 5 \times 10^{12}$ cm; Rau, Greiner & McCollough 2003), similar to the disc radius in V404 Cyg ($R_{out} \approx 9 \times 10^{11}$ cm; Muñoz-Darias et al. 2016) and slightly larger than the disc radii inferred for GRO J1655−40, GRO 1744−28 and GX 339-4 (Shahbaz et al. 1998; Homan et al. 2005). However, given the large difference in BH masses and therefore in the inner-disc radius R_{in}, for HLX-1 this would imply $R_{out} \sim 100 R_{in}$ while for Galactic stellar-mass BHs, $R_{out} \sim 10^5 R_{in}$.

4.2 Disc size from optical continuum fitting

As discussed in Section 2.3, the optical/UV continuum emission in the high and intermediate state must come mostly from an irradiated disc, with the addition of a red excess. Our *diskir* modelling of the 2010 *HST* data together with stacked high/soft *Swift* data (Tables 2 and 3) suggests an outer-disc radius $R_{out} \sqrt{\cos\theta} = (2.2^{+0.6}_{-0.4}) \times 10^{13}$ cm. This is consistent with the outer radii estimated by Farrell et al. (2012) and Soria et al. (2012a), and is a factor of 3 smaller than the value fitted by Farrell et al. (2014); a value $R_{out} \sqrt{\cos\theta} \approx 3 \times 10^{13}$ cm was estimated by Mapelli et al. (2013a) with the irradiated disc model of Patruno & Zampieri (2008). The main reason why our optical radius estimate is on the lower side of the measurement distribution is that we have attributed all the red and near-IR emission in the low-state 2013 *HST* data set to a stellar component rather than the disc (Section 3.2), and have then kept this model component constant in the spectra for the intermediate and high states. This reduces the outer radius of the disc required to fit the optical data.

The effective temperature at the outer edge of the disc (where irradiation dominates over viscous heating) can be estimated from the relation $\sigma [T(R_{out})]^4 \approx (f_{out} \, L_X) / (4\pi R_{out}^2)$, where f_{out} is the reprocessing fraction. From our *diskir* fit for the 2010 *HST* data set, we infer $T(R_{out}) \approx 20\,000$ K. An alternative way of estimating the outer-disc temperature is to fit the 2010 *HST* data points with a single blackbody component, because the irradiated disc emission is dominated by the blackbody emission from the largest annulus. We verified that this method also suggests an outer-disc temperature of $\approx 20\,000$ K (for line-of-sight extinction).

In conclusion, the disc radius derived from optical photometry is at least ≈ 20 times, and more likely 40 times, larger than the radius derived from the X-ray light curve. The two values cannot be reconciled even by taking into account systematic uncertainties in both methods. While the outburst time-scale is within the range of Galactic X-ray binaries, the peak optical brightness of the disc ($M_V \approx -11$ mag) is several magnitudes brighter; the most luminous irradiated discs in Galactic X-ray binaries reach only $M_V \sim -5$ mag

(van Paradijs & McClintock 1994). In Section 5, we will discuss two scenarios that address this discrepancy: either by attributing the optical emission to a circumbinary (CB) disc or by confining the cycle of X-ray outbursts to the innermost rings of the disc.

4.3 Implications for the system parameters

In the absence of dynamical measurements for HLX-1, determining the outer-disc radius provides an important constraint on the binary period and orbital separation, and therefore also on the type of donor star and mass transfer mechanism. Analytical models and numerical simulations suggest that for $q \equiv M_2/M_1 \ll 1$ (where M_1 is the BH mass and M_2 the donor star mass), the disc can extend to the tidal truncation radius R_T:

$$R_{out} \approx R_T \approx 0.60 \, a/(1+q) \tag{9}$$

(Paczyński 1977; Papaloizou & Pringle 1977; Whitehurst 1988; Artymowicz & Lubow 1994; Warner 1995). For the range of mass ratios of interest here ($q \sim 10^{-5}$–10^{-3}), the radius of the donor star (assumed to be filling its Roche lobe) is well approximated by

$$R_2 \approx 0.49 \, a q^{1/3} \tag{10}$$

(Paczyński 1971; Eggleton 1983). Note also that for $q \ll 1$, the companion star fills its Roche lobe at a binary separation $a \approx 2 R_2 q^{-1/3}$, and gets tidally disrupted at a binary separation $a_{td} \approx R_2 q^{-1/3}$ (Rees 1988). The binary separation is related to the binary period via Kepler's third law:

$$a = 1.50 \times 10^{13} (M_1 + M_2)^{1/3} \, P_{yr}^{2/3} \text{ cm}$$
$$= 0.63 \times 10^{13} (M_1 + M_2)_4^{1/3} \, P_d^{2/3} \text{ cm}, \tag{11}$$

where the masses are in units of $M_\odot$ or $10^4 \, M_\odot$, respectively.

Here, we will briefly illustrate the characteristic system parameters corresponding to the two alternative cases of $R_{out} \lesssim 10^{12}$ cm and $R_{out} \approx 2.5 \times 10^{13}$ cm (two representative values for the scenarios discussed in Sections 4.1 and 4.2). We will also assume a BH mass of $\approx (2 \pm 1) \times 10^4 \, M_\odot$.

If it corresponds to the outer-disc radius, the characteristic size derived from the X-ray light curve implies a binary separation $a \lesssim 1.7 \times 10^{12}$ cm (equation 9) and a binary period $P \lesssim 2.3$ h. The Roche lobe radius of the secondary is $R_2 \lesssim 2.3 \times 10^{10}$ cm $\approx 0.33 \, R_\odot$ for $q = 2 \times 10^{-5}$, or $R_2 \lesssim 3.7 \times 10^{10}$ cm $\approx 0.53 \, R_\odot$ for $q = 10^{-4}$. Thus, the inferred constraint on the secondary Roche lobe can only be satisfied by an M-dwarf main-sequence donor star with $M_2 \lesssim 0.4 \, M_\odot$ (Boyajian et al. 2012). However, it is also possible that the donor star has a radius much lower than its initial radius on the main sequence because it has already lost most of its outer envelope as a result of the intense mass transfer. For a Roche lobe-filling secondary star, and $0 < q \lesssim 10^{-3}$, the period–density relation is well approximated by $P \rho^{1/2} \approx 0.41$ (Eggleton 1983), where P is in days and ρ in g cm^{-3}. In our compact scenario for HLX-1, a period of ≈ 2.3 h corresponds to a density $\rho \approx 18$ g cm^{-3}. This is consistent with the density of an M3–M4 main-sequence star (Boyajian et al. 2012).

As discussed in Section 4.2, a small disc of radius $R_{out} \lesssim 10^{12}$ cm inside the BH Roche lobe cannot explain the bright optical emission. Therefore, we propose that the latter component comes from an irradiated CB disc. Smoothed particle hydrodynamics models show (Artymowicz & Lubow 1994) that the inner boundary of a CB disc is truncated by tidal forces at a radius $R_{CB, in}$ varying between $\approx 1.8a$ and $\approx 3a$ depending on orbital eccentricity. The difference is not significant for our case, because the emission dip expected from this gap falls in the far-UV band, where we do not have

any measurements. Copperwheat (private communication) used his code (Copperwheat et al. 2005, 2007) to simulate irradiated disc spectra with or without a gap, and we verified that the difference is undetectable with the available X-ray and optical data points. The outer radius of the irradiation-dominated CB disc would have to extend to $R_{CB,out} \gtrsim 15a \approx 2.5 \times 10^{13}$ cm to reproduce the optical continuum; its continuum emission spectrum would look essentially identical to the spectrum of an irradiation-dominated accretion disc of the same size ($T(R) \propto R^{-1/2}$). See also Farris et al. (2014, 2015), Yan et al. (2015), D'Orazio et al. (2016), D'Orazio, Haiman & Mac-Fadyen (2013), Roedig, Krolik & Miller (2014) and Artymowicz & Lubow (1996) for further modelling of CB disc structure and emission.

Observational evidence for mid-infrared emission from a dusty CB disc illuminated by the compact X-ray source has been found in several X-ray binaries, such as the Galactic BH candidates GRS 1915+105 (Rahoui et al. 2010), A0620−00 and XTE J1118+480 (Muno & Mauerhan 2006). Among ULXs, a CB disc was proposed for Holmberg IX X-1 (Dudik et al. 2016) and Holmberg II X-1 (Lau et al. 2017). A CB disc fed by outflows through the L2 point is also likely to be present in SS 433, based on optical spectroscopic studies of its stationary Hα, Brγ, Paschen and He I emission lines (Blundell, Bowler & Schmidtobreick 2008; Perez & Blundell 2009, 2010; Bowler 2013). From the rotational velocity shift of the red and blue line components, the characteristic emitting radius of the SS 433 CB disc is $\sim 10^{13}$ cm (Bowler 2013). We have argued that in the CB disc scenario for HLX-1, its characteristic radius would also be $\sim 10^{13}$ cm; however, its irradiating luminosity at outburst peak would be much higher than in SS 433, and would keep the CB disc in the hot, optically thick state with significant contributions to the UV continuum emission.

Let us now assume instead that the outer accretion disc radius is $R_{out} \approx 2.5 \times 10^{13}$ cm, based on the optical continuum measurements. Following the same argument, for $q \ll 1$ and $M \approx 2 \times 10^4 \, M_\odot$, this disc radius implies a binary separation $a \approx 4 \times 10^{13}$ cm and a binary period $P \approx 12$ d. The Roche lobe radius of the secondary is $R_2 \approx 5.5 \times 10^{11}$ cm $\approx 8 \, R_\odot$ for $q = 2 \times 10^{-5}$, or $R_2 \approx 9.5 \times 10^{11}$ cm $\approx 14 \, R_\odot$ for $q = 10^{-4}$, or $R_2 \approx 2.0 \times 10^{12}$ cm $\approx 29 \, R_\odot$ for $q = 10^{-3}$. From the period–density relation for $0 < q \lesssim 10^{-3}$, we obtain a mean density $\rho \approx 1.2 \times 10^{-3}$ g cm^{-3}. This is consistent with several types of evolved stars (e.g. blue supergiants, Hertzsprung gap stars, red giants). Massive stars in the last stages of stellar evolution are much more likely sources of continuously high mass transfer rate (for time-scales of a few 10^5 yr) than a main-sequence M star. The only circumstance in which an M star can provide the required mass transfer rate is if it is currently undergoing tidal stripping of its envelope. Therefore, we conclude that the large-disc scenario is much more consistent with the observations. This scenario would also imply that HLX-1 is fuelled in a way similar to ULXs, despite the likely large difference in the mass of the accretor. For completeness, in Section 5, we will outline possible outburst mechanisms both for the case of a smaller and of a larger orbital separation, keeping in mind that the latter case is more likely to apply to HLX-1.

5 WHAT IS THE OUTBURST MECHANISM?

5.1 Summary of HLX-1 outburst models proposed in the literature

The fast outburst rise and subsequent exponential decay, and the harder power-law spectrum in the low states, can be qualita-

tively explained with the disc-instability model usually applied to X-ray binaries (Hameury et al. 1997, 1998; Dubus et al. 1999; Lasota 2000, 2001, 2008; Menou et al. 2000; Dubus, Hameury & Lasota 2001; Lasota, Dubus & Kruk 2008). In the model, the accretion disc extends to the innermost stable circular orbit R_{isco} when in the high state. Instead, in the low state, the disc is truncated at $R_{tr} (\gg R_{isco})$, within which the hot inflow is radiatively inefficient and geometrically thick. Moreover, in the low state, all disc annuli are on the cold branch of the density–temperature S-curve (characterized by neutral hydrogen and low viscosity), with inflowing matter piling gradually till the surface density exceeds the critical density. This occurs at R slightly larger than R_{tr}, from where a heating front propagates outwards (an inside-out outburst). The increased viscosity and accretion rate cause the inner disc to extend inwards towards R_{isco}, and the system enters a high state, where the entire disc is on the hot branch of the S-curve. When the outburst subsides and the accretion rate diminishes, the outer disc cools down and the inner disc evaporates, creating a radiatively inefficient, optically thin, geometrically thick inflow.

However, it was soon realized that this model does not work well for HLX-1 (Lasota et al. 2011). The observed X-ray luminosity of $L_X \approx 2$–4×10^{40} erg s^{-1} during the low/hard state (Servillat et al. 2011; Yan et al. 2015) requires an accretion rate larger than a few 10^{20} g s^{-1} in the hot, radiatively inefficient inner region, and hence $\dot{M}(R_{tr}) \gtrsim$ a few 10^{20} g s^{-1}. This implies that starting from a low-density disc in the cold state, the transition radius at which the disc becomes hot is $R_{tr} \approx 2 \times 10^{13}$ cm (Dubus et al. 2001; Lasota 2008). If the inner disc was truncated at this large radius, it would take $\sim 10^2$ yr to refill before it extends again to R_{isco}. The high state would then also be expected to last for hundreds of years, which is contradicted by the observed rapid recurrence times and short outbursts. The disc-instability model predicts $\dot{M}(R) \propto R^{2.65}$ in the low state (Lasota 2001). If we impose a smaller truncation radius in the low state, $R_{tr} \lesssim 10^{12}$ cm, to reconcile the refill time with the observed time-scales, and $\dot{M}(R_{tr}) \approx$ a few 10^{20} g s^{-1}, we obtain $\dot{M}(R_{out}) \sim 10^{24}$ g s^{-1} $\sim 10^{-2} \, M_\odot$ yr^{-1}, a value completely unphysical for a donor star. Moreover, the ratio between inter-outburst and outburst luminosity in HLX-1 is $\approx 3 \times 10^{-2}$, about five to six orders of magnitude higher than the ratios observed in transient BH X-ray binaries and predicted by the disc-instability model. In summary, despite certain qualitative similarities in the temporal and spectral properties of HLX-1 and BH low-mass X-ray binaries, the disc-instability model fails to account for the time-scales of HLX-1's outburst duty cycle and low/hard state luminosity of $L_X \sim 10^{40}$ erg s^{-1}.

One may explain the repeat of the first few outbursts at almost the same time interval of ≈ 1 yr as successive bursts of mass transfer from a donor star each time it passes through periastron of a very eccentric orbit (Lasota et al. 2011). Taking the binary period as 1 yr, the fitted BH mass of $\sim 10^4 \, M_\odot$ then sets the orbital semimajor axis $a \approx 3 \times 10^{14}$ cm (≈ 20 au). On the other hand, the small disc size required by the fast rise and decay (radius $\lesssim 10^{12}$ cm) constrains the distance at the periastron, and hence the orbital eccentricity. The best solutions correspond to extremely high elliptical orbits (almost reaching the parabolic limit; Lasota et al. 2011; Soria 2013). Such systems would be short-lived and/or unstable, as the entire envelope of the donor star would be completely stripped after a few periastron passages. A less extreme alternative was proposed (Miller, Farrell & Maccarone 2014), with an orbital eccentricity of 'only' ≈ 0.9, where the mass transfer occurs via wind capture, resulting in a lower specific angular momentum for the inflowing gas and hence a shorter accretion time-scale. This scenario still cannot avoid the donor star to be tidally stripped.

Crucially, the recurrence time has increased substantially in the latest outbursts, up to 470 d between the rise of the last two outbursts in 2013–2015 (Yan et al. 2015), and it has been a couple of years since the start of the last outburst in January 2015. The periastron-passage scenario has to account for this development. Change in the orbital period can happen in highly eccentric, extreme mass-ratio systems undergoing mass-loss and/or mass redistribution. The study of Godet et al. (2014) has shown that a donor star captured by an IMBH on an orbit with $e \gtrsim 0.9998$ and periastron distance between ≈ 2 and 3 times the tidal disruption radius could reach a minimum period of about 1 yr after a few dozen orbits. The star would lose a few per cent of its mass at each passage, leading to a rapid increase in the orbital period, and eventually what is left of the star becomes unbound after only two or three more orbits. This is consistent with the observations and perhaps explains why there has been no outburst since 2015.

Smoothed particle hydrodynamics simulations of a similar scenario (but with different assumptions on orbital eccentricity, mass-loss rates and viscosity) by van der Helm, Portegies Zwart & Pols (2016) showed that more moderate eccentricities such as $e = 0.7$ or even $e = 0.95$ are not sufficient to reproduce the rapid change in the recurrence time-scale.

An important feature of all models based on extremely high eccentricity and tidal stripping is that the accretion disc must be small, with a maximum size comparable to the periastron distance, in agreement with the X-ray time-scales rather than with the optically measured size. That means that such models require an additional optically thick, irradiated gas region to account for the optical/UV continuum. For a similar reason, we have suggested the presence of a CB disc in the case of a compact system (Section 4.3). However, the CB disc scenario would itself have serious troubles, in the case of a highly eccentric orbit. In that situation, the apastron distance would determine the size of the gap between inner disc and the CB disc; therefore, the inner radius (hottest part) of the CB disc would have to be located at a distance $\gtrsim 3 \times 10^{14}$ cm, if the semimajor axis of the orbit is large enough to correspond to a binary period of ≈ 1 yr (from Kepler's law). At those distances, the irradiated CB disc would be too cold to produce the observed UV/optical emission. Thus, a highly eccentric orbit would require an alternative, more complicated distribution of irradiated gas closer to the BH, possibly a transient combination of accretion streams, tidal streams and outflows around the stripped donor star. The high-eccentricity, periastron-passage mass transfer scenario also implies that our chance detection of HLX-1 as a hyperluminous X-ray source is a one-off event in the system's evolutionary history, associated with a recent capture and rapid shredding of a donor star (on a time-scale of a few years). HLX-1 should now head into quiescence.

Instead, here we want to consider whether HLX-1 can be a more stable system, capable of supporting high mass transfer for a much longer time-scale (e.g. $\sim 10^5$ yr rather than ~ 10 yr). For this, we need to discard the assumption that the outburst recurrence time-scale is approximately the same as the orbital period. We will discuss and compare two alternative physical mechanisms that may produce outburst cycles, not based on the disc-instability scenario: one for the case of a small orbital separation, and one for a larger separation (consistent with the optical disc size measured in HLX-1). As we explained in Section 4.3, we will argue that the latter one is the more plausible.

5.2 A mass transfer instability scenario for the small-disc case

The first scenario assumes a small accretion disc with an outer radius $\lesssim 10^{12}$ cm. The observed time-scale for the luminosity decline corresponds to the time needed for the whole disc to drain, and the outburst is due to an intermittent or variable gas inflow. Without the aid of a highly eccentric orbit, an alternative mechanism is needed for the recurrent bursts of mass transfer from the donor star. Given the strong X-ray luminosity and small orbital separation, irradiation on the donor star is expected to be strong. Studies (Phillips & Podsiadlowski 2002) have shown that the pressure exerted by a strong irradiation could press down the surface of the star, causing a temporary loss of contact with the critical Roche surface at the inner Lagrangian point (L1). When this happens, the star loses mass instead through the outer Lagrangian point (L2), feeding a CB disc. However, moderate irradiation by X-rays could have an opposite effect: irradiative heating may lead to an increase in the donor star's atmospheric scaleheight, resulting in more mass flowing into the BH's Roche lobe through L1 (Kovetz, Prialnik & Shara 1988; Podsiadlowski 1991). The importance of irradiation feedback in BH X-ray binaries (especially those with a large accretion disc, which casts a shadow on the star) has been under debate (Vilhu, Ergma & Fedorova 1994; Ritter, Zhang & Kolb 2000; Ritter 2008), but observations have shown that the process does operate in binary systems containing a white-dwarf accretor (Mróz et al. 2016). Persistent X-ray irradiation could drive cycles of high and low mass transfer rates in low-mass X-ray binaries, with peaks reaching 10^{-5} M$_\odot$ yr^{-1} or higher (Harpaz & Rappaport 1994), but the characteristic duty cycle of $>10^4$ yr implies that this mechanism is irrelevant for the outbursts seen in HLX-1.

With the effects of radiation pressure on the donor star surface in mind, we suggest the following scenario to account for the ~ 100 d HLX-1 outburst cycles. At the peak of each outburst, the irradiating X-ray pressure becomes high enough to press down the donor star's atmosphere, making the star detach from the critical Roche surface at L1. When the disc is not fed, the outburst subsides on the viscous time-scale. After most of the disc is consumed, the system enters a low/hard state, with a luminosity allowing the donor star to regain contact with the critical Roche surface and resume the mass transfer process. This sequence of events explain the presence of a CB disc (required to account for the optical luminosity), presumably fed through L2 at the moment that the star becomes detached at L1, in a natural manner. This scenario works when the X-ray luminosity $L_X \gtrsim 0.8 L_{Edd,2}$ (Phillips & Podsiadlowski 2002), where $L_{Edd, 2}$ is the Eddington luminosity of the star. For HLX-1, $L_X \approx 10^{42}$ erg s^{-1} during the outburst peak. Such luminosity is $\gg L_{Edd, 2} \approx 10^{38}$ erg s^{-1}. The question is how much accretion luminosity reaches L1 in the presence of shadowing from the outer edge of the disc. There are several possibilities for a partial irradiation of L1 even in the presence of a disc shadow (Viallet & Hameury 2008). For instance, a warped disc may provide the amount of irradiation needed. Accretion discs in both the high/soft state and the super-Eddington regime could launch strong winds (Neilsen & Lee 2009; Ponti et al. 2012; Muñoz-Darias et al. 2016; Pinto et al. 2016), which can scatter a fraction of the X-ray emission down towards L1. Photons can also be scattered towards L1 by an extended hot corona above the inner disc or near the base of a jet. Note that for this to happen, the vertical extent of the X-ray scattering region would have to be $\gtrsim 10^{11}$ cm, for a disc with a thickness $H/R \sim$ a few 10^{-2}. From the observed temperatures and luminosities of outer discs in the Galactic X-ray binaries, Viallet & Hameury (2008) estimated

that about $\sim 10^{-3}$ of the accretion luminosity could be scattered by the disc wind, outflow or corona to irradiate the region near L1. The condition $L_1 \gtrsim 0.8 L_{\mathrm{Edd},2}$ is thus easily satisfied, leading to the detachment of the donor star from the critical Roche surface at L1. As a comparison, the Galactic source SS 433 is an example of an X-ray binary where the direct emission is partially occulted or eclipsed, but a residual hard X-ray component (multi-temperature bremsstrahlung and/or Compton scattering emission) is seen even when the disc is eclipsed by the companion star. The inferred emission region for this extended component is $\sim 10^{12}$–10^{13} cm (Kotani et al. 1996; Cherepashchuk et al. 2007; Krivosheyev et al. 2009; Kubota et al. 2010; Marshall et al. 2012), which is as large as or larger than the size of the accretion disc ($R_{\mathrm{out}} \approx 2 \times 10^{12}$ cm; Gies, Huang & McSwain 2002). The observed X-ray luminosity of SS 433 ($L_{\mathrm{X}} \approx 10^{36}$ erg s^{-1}) is $\sim 10^{-3}$–10^{-4} times the true luminosity (Medvedev & Fabrika 2010; Fabrika et al. 2015; Khabibullin & Sazonov 2016), because only a small fraction of X-rays are scattered at all angles by the outflow while most of the radiation is emitted inside the polar-axis funnel (Medvedev & Fabrika 2010; Atapin et al. 2015). If a similar fraction of the X-ray luminosity is scattered by a wind above the disc plane in HLX-1, the pressure exerted by the irradiation flux would satisfy the condition given in Phillips & Podsiadlowski (2002) and cause an intermittent mass transfer.

In conclusion, we stress that the scenario described in this section is not the most likely explanation for HLX-1, but we have presented it for completeness, as an example of an at least theoretically possible cycle of variability in a highly luminous, compact system, with a donor star alternatively feeding the inner disc and the CB disc.

5.3 An oscillating wind scenario for the large-disc case

The second scenario considers a system with an accretion disc extending to $R_{\mathrm{out}} \gtrsim 10^{13}$ cm. The arguments outlined in Section 5.2, about irradiation suppressing mass transfer through L1 and inducing L2 overflow (Phillips & Podsiadlowski 2002), are also applicable here. The larger binary separation in this case is compensated by a larger cross-section for photon interception provided by the larger donor star. The larger orbital separation implies that the Roche lobe (Section 3.3.2) can accommodate a more massive donor, and hence permits a higher value for $L_{\mathrm{Edd},2}$; in principle, this makes it harder for the irradiation condition to be satisfied. However, in the large-disc scenario, the condition is irrelevant and cannot explain the outburst cycle of HLX-1. Here is the reason: The amount of material stored in a steady-state standard disc with $R_{\mathrm{out}} \sim 10^{13}$ cm is a few 10^{30} g (equation 4), but only a few 10^{28} g are accreted into the BH during each outburst (Section 4.1 and Yan et al. 2015). The large outer disc practically is a reservoir that tends to smooth out mass transfer fluctuations from the donor star on time-scales shorter than the fluid viscous time-scale at the outer radius (which is $\sim 10^3$ yr). Whether or not the donor star temporarily detaches from L1 during each outburst cycle is therefore unimportant, when the amount of mass involved in each outburst duty cycle is only a small fraction of the mass stored in the disc. The main feature of the large-disc scenario is that the outburst would terminate when a small part of the disc (presumably, the innermost part) is depleted. Thus, the observed alternation of high and low states must be driven by changes in the accretion rate through the disc at $R \lesssim 0.1 R_{\mathrm{out}}$ rather than by variations in the mass transfer through L1.

A comparison of the outburst behaviours of HLX-1 and of the Galactic BH V404 Cyg (Kimura et al. 2016) shows some interesting

similarities. The binary parameters of V404 Cyg suggest that the accretion disc has a radius $R_{\mathrm{out}} \approx 9 \times 10^{11}$ cm. It is believed that during the outburst a massive thermal wind is launched, depleting the accretion disc; the wind is strong enough to deplete the mass inflow (Muñoz-Darias et al. 2016). As a result, the inner-disc region (within a radius $R \sim 0.1 R_{\mathrm{out}}$) is no longer fed (or is fed at much lower rates) by the mass inflow from larger radii. The outburst subsides on the viscous time-scale of the inner part of the disc (inside the wind depletion radius), which is much shorter than the viscous time-scale of the whole disc. An estimate of only ≈ 0.1 per cent of the disc mass is accreted during an outburst (Muñoz-Darias et al. 2016). The optical continuum is mostly reprocessed emission from the irradiated surface of the full accretion disc. A consequence of the massive disc outflow is the formation of a large Hα-emitting nebula. These features of V404 Cyg are qualitatively similar to what we observe in HLX-1.

Another property that V404 Cyg and HLX-1 have in common is the relatively high luminosity in the inter-outburst periods. At $L_{\mathrm{X}} \approx 10^{33}$ erg s^{-1}, V404 Cyg is two orders of magnitude more luminous than typical BH X-ray binaries in quiescence (Armas Padilla et al. 2014; Muñoz-Darias et al. 2016; Rana et al. 2016). Even so, the ratio of outburst to inter-outburst luminosities is still as high as $\sim 10^5$ in V404 Cyg, while it is only ≈ 30 in HLX-1. The anomalously high luminosity in the inter-outburst periods can be explained by the continuing presence of low-level accretion from the already detached outer disc, which is not completely depleted after the outburst and is working as a reservoir (Muñoz-Darias et al. 2016). In V404 Cyg, the double-peaked Hα emission line in the inter-outburst period is strong evidence that the outer disc survives through quiescence (Muñoz-Darias et al. 2016). In this scenario, the different ratio of outburst to inter-outburst luminosities suggests that the wind-driven disruption of the inner accretion flow is not as strong in HLX-1 as it is in V404 Cyg.

If the disc wind is strong enough to play a major role in regulating the outbursts of HLX-1, a damped disc wind instability (Begelman, McKee & Shields 1983; Shields et al. 1986) would be inevitable. This instability occurs when accretion, at a rate $\dot{M}_{\mathrm{a}}$ in the X-ray emitting region of the disc, triggers a massive wind in a larger annulus of the disc (at $R \equiv R_{\mathrm{w}} < R_{\mathrm{out}}$), with an outflow rate $\dot{M}_{\mathrm{w}}(t) \equiv C \dot{M}_{\mathrm{a}}(t)$, with $C \gtrsim$ a few. For this to happen, the wind has to be directly induced by irradiation. The original model put forward by Begelman et al. (1983) and Shields et al. (1986) considered a thermal (Compton) wind, but the mechanism would also work with a radiatively driven wind. In a steady state, $\dot{M}_{\mathrm{in}} = \dot{M}_{\mathrm{a}} + \dot{M}_{\mathrm{w}} = (1 + C) \dot{M}_{\mathrm{a}}$, where $\dot{M}_{\mathrm{in}}$ is the accretion rate in the outer region of the disc beyond the wind-dominated region. A small positive perturbation $\delta \dot{M}_{\mathrm{a}}$ will cause a prompt increase $\delta \dot{M}_{\mathrm{w}} = C \times \delta \dot{M}_{\mathrm{a}}$ of the outflow rate. As a consequence, $\dot{M}_{\mathrm{in}} < \dot{M}_{\mathrm{a}} + \dot{M}_{\mathrm{w}}$, and the disc is depleted inside R_{w}. While the wind immediately reacts to the X-ray luminosity increase, it takes a viscous diffusion time-scale for $\dot{M}_{\mathrm{a}}$ to feel the effect of the depleted inflow arriving from R_{w} and to re-adjust to a lower value. When that happens, the wind immediately decreases, so that $\dot{M}_{\mathrm{in}} > \dot{M}_{\mathrm{a}} + \dot{M}_{\mathrm{w}}$ and the inner disc builds up again. It is the difference in the response time-scales of the radiation-induced wind and of the inner-disc accretion that creates and sustains the oscillations. If $C \gtrsim 10$, oscillations are persistent; for $1 < C \lesssim 10$, they are damped after a few cycles (Shields et al. 1986). The amplitude of the oscillations is $\dot{M}_{\mathrm{a,max}}/\dot{M}_{\mathrm{a,min}} \approx 10$ (Shields et al. 1986). Using the standard Shakura–Sunyaev viscosity parametrization, Shields et al. (1986) found an oscillation period $P_{\mathrm{osc}} \sim 0.1$–$0.4\,\tau_{\mathrm{w}}$, where τ_{w} is the viscous time-scale in the wind region. The period increases when the

wind efficiency parameter C decreases, but is only a weak function of C.

We suggest that this model is applicable to HLX-1, which is expected to have strong disc winds in outburst. As a comparison, Galactic low-mass X-ray binaries in the high state, with $L_X \sim 0.1 L_{Edd}$, can have a mass outflow rate in a disc wind $\sim$1–20 times the accretion rate (Díaz-Trigo & Boirin 2016), which is strong enough to allow the wind instability described above to develop. However, we need to estimate whether the wind instability predicts the correct outburst time-scale.

For a thermal wind, the launching radius is $R_w \sim 0.1 R_{IC}$ (see Shields et al. 1986), where R_{IC} is the Compton radius, where the isothermal sound speed of the gas equals the escape velocity from the disc. For an irradiating source spectrum peaking at energies ≈ 1 keV($\approx 10^7$ K), the Compton radius $R_{IC} \sim 10^{11}(M/M_\odot)$ cm. Therefore, in HLX-1, thermal winds could only be launched if the disc extended to $\sim 10^{14}$ cm, which does not appear to be the case. However, when the effect of radiation pressure is also included, strong winds can be launched from smaller radii: in particular, Proga & Kallman (2002) showed that UV lines can drive powerful winds from regions of the disc that have a surface temperature $\lesssim 50\,000$ K. Based on the results of our broad-band modelling, we have estimated (Section 4.2) an effective temperature $T_{eff} \approx 20\,000$ K at $R \approx R_{out} \approx (2 \times 10^{13})/\sqrt{\cos\theta}$ cm in the high state. In the irradiation-dominated part of the disc, $T_{eff} \propto R^{-1/2}$ (Dubus et al. 1999). Thus, we expect a temperature $T_{eff} \approx 50\,000$ K at $R \approx R_w \approx 3 \times 10^{12}$ cm $\approx 3 \times 10^{-3} R_{IC}$. [As a comparison, for X-ray binaries $R_w \sim 5 \times 10^{-2} R_{IC}$, and for AGN, $R_w \sim 10^{-4} R_{IC}$ (Proga & Kallman 2002).]

Assuming a Shakura–Sunyaev disc (Shakura & Sunyaev 1973; Frank et al. 2002) with Kramer's opacity and $\dot{M} \sim 10^{21}$–10^{22} g s^{-1} (spanning the range of plausible accretion rates for HLX-1 in the low and high state), we obtain a viscous time-scale $\tau \sim$ a few years at $R \sim$ a few 10^{12} cm. (This can be verified simply by recalling that $\tau \sim [\alpha\,\Omega\,(H/R)^2]^{-1} \approx 6$ yr for $(H/R) \approx 0.01$, $\alpha \approx 0.3$, $M \approx 2 \times 10^4$ M$_\odot$.) Therefore, the wind oscillation period P_{osc} can be as short as ≈ 1 yr (Shields et al. 1986). The observed outburst duty cycle in HLX-1 is consistent with this scenario. The increase in the outburst recurrence period, accompanied by a reduced fluence in each cycle (Yan et al. 2015), is also consistent with damping of the oscillations, as the wind multiplication factor decreases.

Line-driven winds are effective when the UV luminosity $L_{UV} > L_{Edd}/M_{max}$ (Murray et al. 1995; Proga, Stone & Drew 1998; Proga & Kallman 2002), where M_{max} is the limit of the force multiplier, which can be as high as ≈ 2000 for low-ionization gas. In the case of HLX-1, for the 2010 high/soft state spectrum, we infer an unabsorbed luminosity in the 13.6–100 eV band $L_{UV} \approx 0.15 L_X \sim$ a few $10^{-2} L_{Edd}$. Therefore, we can at least say that there are enough UV photons available in the system to drive a strong wind. However, the amount of mass carried in the wind depends on the ionization parameter of the gas, and hence on the amount of shielding from direct X-ray irradiation, which would overionize the wind and reduce the effectiveness of line driving. We do not have any empirical constraints on the wind parameters for HLX-1, perhaps because our line of sight is almost face-on, not intersecting the wind. Thus, a more detailed modelling of the energetics of the wind is beyond the scope of this work. However, we do note that optical spectra of HLX-1 have shown an Hα emission line with a luminosity of a few 10^{37} erg s^{-1} and full width at half-maximum of ≈ 400 km s^{-1} (Wiersema et al. 2010; Soria et al. 2013). The line is too narrow to be directly associated with a disc wind, but it suggests at least the presence of diffuse gas around the system.

A wind-driven sinusoidal oscillation in $\dot{M}_a$ does not necessarily result in a sinusoidal oscillation in L_X, because accreting BHs have distinct accretion states, and hysteresis in their cycle of states. If $\dot{M}_a$ exceeds a few per cent of $\dot{M}_{Edd}$ at the peak of the oscillation, the system will switch to the high/soft state, before returning to the low/hard state during the low part of the oscillation. The fact that the time spent in the high/soft state was getting shorter from cycle to cycle (Yan et al. 2015), and no new outbursts have been detected for a couple of years (since 2015 January), may both be a consequence of the damping of the oscillation. We suggest that the system is now settled in the low/hard state, where the long-term-average accretion rate is below the state-transition threshold of a few per cent of the Eddington accretion rate, and the damped oscillation in $\dot{M}_a$ does not reach the threshold for a hard-to-soft state transition any more. For example, we suggest a scenario in which the long-term-average accretion rate is $\approx 0.05 \dot{M}_{Edd} \approx 10^{21}$ g s^{-1} $\approx 2 \times 10^{-5}$ M$_\odot$ yr^{-1} (for an efficiency $\eta \approx 0.1$), just below the threshold for the collapse of the hot, radiatively inefficient corona and the resulting hard-to-soft transition. By analogy with Galactic X-ray transients, the radiative luminosity in this state is expected to be $\approx 0.02 L_{Edd} \approx 4 \times 10^{40}$ erg s^{-1} (consistent with the luminosity inferred from *Swift* since the end of the last outburst), with an additional similar contribution to the accretion power in the form of kinetic power of a jet.[2] A positive perturbation in the accretion rate would push the system over the threshold for the high/soft state at $L \sim 0.1 L_{Edd}$ (briefly peaking at $L \approx 0.3 L_{Edd}$ for a few days after the transition). The subsequent wind-driven oscillation of the accretion rate below $\approx 0.02 \dot{M}_{Edd}$ would bring the system back to the hard state.

An accretion rate $\dot{M} \approx 10^{21}$ g s^{-1} is very high but comparable to the accretion rates proposed for the Galactic source SS 433 and for the most powerful ULXs in nearby galaxies (Feng & Soria 2011; Sutton, Roberts & Middleton 2013; Fabrika et al. 2015; Bachetti 2016), which are thought to be super-Eddington, stellar-mass accretors. For a 10 M$_\odot$ BH, an accretion rate $\dot{M} \approx 10^{21}$ g s^{-1} corresponds to $\dot{m} \equiv \dot{M}/\dot{M}_{Edd} \approx 100$ and a luminosity $L \approx (1 + 0.6 \ln \dot{m}) \approx 4 L_{Edd} \approx 5 \times 10^{39}$ erg s^{-1} (Poutanen et al. 2007). In HLX-1, for a BH mass $M \approx 2 \times 10^4$ M$_\odot$ and a binary separation $a \approx 4 \times 10^{13}$ cm (Section 3.3.2), the binary period is $P \approx 10$ d. A donor star of mass $M_2 \approx 15$ M$_\odot$ is able to fill its Roche lobe at a radius $R_2 \approx 25$ R$_\odot$ (typical of a blue supergiant). In summary, this scenario does not require that we are *observing* the system during a one-off, short-duration event, such as the tidal stripping of a recently captured star over a few orbital time-scales. The average mass transfer rates can instead be sustained for $\sim 10^5$ yr (or $\sim 10^4$ for a red giant donor). It still does require peculiar *formation* conditions, such as a donor star in a close orbit around an IMBH, filling its Roche lobe as it evolves off the main sequence. The likelihood of such event is hard to estimate with the constraints at hand, and not knowing what fraction of compact stellar systems contains an IMBH in their core [Caputo et al. (2017) estimate the existence of $\sim 10^6$ IMBHs with masses $\sim 10^4$ M$_\odot$ within 100 Mpc]. On the other hand, from the observational point of view, HLX-1 is a unique system within at least 100 Mpc, and we should not discount one-off events. If our oscillation scenario is correct, we predict that the X-ray luminosity of HLX-1 over the next few years will remain at $\gtrsim 10^{40}$ erg s^{-1}; instead, if short-duration

---

[2] Here, we have assumed that the low/hard state is less radiatively efficient than the high/soft state: $\eta_{lh} \approx 0.05$ at $\dot{M} \approx 0.05 \dot{M}_{Edd}$, with a similar amount of power going into the jet.

tidal stripping scenarios are correct, HLX-1 should soon fade into quiescence.

6 CONCLUSIONS

We compared the optical/UV brightness of HLX-1 during three sets of *HST* observations taken at different times during the outburst cycle. We fitted the optical/UV data together with X-ray data taken at similar phases, to quantify how the optical/UV luminosity is a function of the X-ray flux. We showed that the optical/UV emission is well modelled with at least two components: a blue component, strongly dependent on the irradiating X-ray flux, and a constant red component. The latter is consistent with an underlying old stellar population, perhaps a globular cluster or the nucleus of a satellite dwarf. The bluer optical emission is dominated by an irradiated disc with an outer radius $R_{out}\sqrt{\cos\theta} \approx 2 \times 10^{13}$ cm. The high level of irradiation of the outer accretion disc disfavours models based on strongly beamed X-ray emission [as proposed by King & Lasota (2014) if HLX-1 were a highly super-Eddington stellar-mass accretor], or at the very least it would require a peculiar wind structure in the polar funnel, in order to scatter a significant number of photons on to the outer disc. The data are also consistent with an additional blue component coming from a young stellar population. The residual optical emission in the 2013 observations (when both the X-ray source and the optical counterpart were at their faintest level) clearly places an upper limit to the (constant) contribution of the young stellar population: we find that a single-population young stellar cluster must have a mass $\lesssim 10^4$ M$_\odot$ to avoid exceeding the blue luminosity in the 2013 data.

From our analysis and comparison of *XMM–Newton* and *Swift* light curves and spectra, we argued that the 2012 November observations were fortuitously taken right at the time of the hard-to-soft transition at the end of an outburst cycle. As a result, based on the analogy with similar transitions in Galactic X-ray transients, we argued that the X-ray luminosity at that point was $\approx(2 \pm 1)$ per cent of the Eddington luminosity. Combining this constraint with the independent constraint on the inner-disc size from spectral fitting ($R_{in}\sqrt{\cos\theta} \approx 50\,000$ km), we estimated a BH mass $\approx(2^{+2}_{-1}) \times 10^4$ M$_\odot$, with a spin parameter $a/M \gtrsim 0.9$ for a moderately face-on viewing angle. This is in agreement with the results of Davis et al. (2011) based only on detailed spectral modelling of the disc spectrum in the high state. For these system parameters, the peak observed luminosity in the high/soft state is $L_X \approx 0.2$–$0.4 L_{Edd}$ (similar to most Galactic BH transients), and the luminosity in the low/hard state is $L_X \approx 0.01 L_{Edd}$. With a different assumption of the geometry of emission in the intermediate state (isotropic rather than disc-like), we obtain a slightly different BH mass, $M \approx (3^{+3}_{-1}) \times 10^4$ M$_\odot$, but the qualitative result is the same: the system oscillates between sub-Eddington, canonical high/soft and low/hard states.

We then discussed the size of the accretion disc, based on two apparently contradicting pieces of information. The short time-scale of the X-ray rise, decay and recurrence time points to a small disc, with $R_{out} \lesssim 10^{12}$ cm, and more likely $\sim$a few $\times 10^{11}$ cm. Instead, the reprocessed UV/blue emission requires a surface with a radius $R_{out} \gtrsim 2 \times 10^{13}$ cm. To reconcile the two observations, we presented and compared two alternative scenarios, both based on a two-zone structure for the accretion flow: an inner region ($\lesssim 10^{12}$ cm) that drives the X-ray outburst and an outer region ($\gtrsim 2 \times 10^{13}$ cm) that produces most of the optical/UV luminosity. In the first scenario, the inner region is the accretion disc inside the BH Roche lobe, and the outer region is a CB disc, with a gap in between due to

the orbit of the donor star. The outburst may be triggered by a mass transfer instability due to the high irradiation seen by the donor star. The star would alternately feed the accretion disc (through the Lagrangian point L1) or the CB disc (through L2) depending on the irradiation condition. In the second scenario, both X-ray and optical/UV emission come from a large accretion disc. However, only the inner region of this inflow produces the X-ray outburst cycles on a short time-scale; the outer disc acts as a long-term reservoir of matter. In this scenario, the mass accretion flow towards the inner region oscillates due to the feedback effect (wind instability) of radiatively driven outflows, which deplete the middle region of the disc and regulate the flow that goes past a radius $\sim 10^{12}$ cm. The latter scenario is similar to the current interpretation of the outburst in the Galactic BH V404 Cyg.

Based on the available optical/UV and X-ray luminosity alone, it is not possible directly to rule out either scenario. The SED expected from an irradiated CB disc is similar to the one expected from an irradiated outer disc of similar size (in both cases, $T \propto R^{-1/2}$). The only difference would be the presence and size of a gap at $R \approx 10^{12}$ cm in the case of a CB disc, due to the orbit of the donor star. The gap would affect disc annuli with a temperature $T_{eff} \approx 10^5$ K, and would produce a small decrease in the far-UV flux, a spectral band that is not directly observable. However, the two scenarios have very different implications for the size and type of donor star and for the binary period. A binary separation of ≈ 1–2×10^{12} cm (small-disc scenario) implies a binary period of only ≈ 2–3 h and a very small Roche lobe for the donor star, consistent only with the size and density of an M-dwarf close to its tidal disruption limit. A large-disc scenario implies a more plausible binary period ~ 10 d, and the secondary Roche lobe can accommodate a blue supergiant or other types of post-main-sequence stars, able to provide a higher mass transfer rate over a longer time-scale. If the donor star is a blue supergiant, this would confirm the presence of a small population of young stars around the IMBH, but the data do not rule out an older donor (ascending the red giant branch). Based on these arguments, we conclude that the large-disc scenario with wind-driven oscillations in the inner region is more consistent with the data and is the most plausible explanation for HLX-1.

More generally, the wind-driven oscillation scenario provides a relatively unexplored mechanism for the generation of super-orbital X-ray variability (in the case of HLX-1, with a super-orbital period ≈ 40 times longer than the binary period), in alternative to the inner-disc/jet precession scenario. We speculate that the same mechanism may explain other examples of super-orbital periodicities in luminous X-ray binaries (Farrell, Sood & O'Neill 2006; Farrell, Barret & Skinner 2009a) and ULXs (e.g. the 115 d periodicity in NGC 5408 X-1; Strohmayer 2009; Foster, Charles & Holley-Bockelmann 2010; Grisé et al. 2013).

According to our adopted scenario, the system is now in the low/hard state at $L_X \sim 10^{-2} L_{Edd}$, only a factor of a few below the accretion rate and luminosity at which we expect a transition to the high/soft state. We suggest that the oscillations in the accretion rate have damped to the point where even at its peak, $\dot{M}$ is no longer high enough to trigger the transition. We do not have empirical evidence to test the origin of the perturbation that caused the damped oscillatory behaviour over the last decade – it could be related to the evolution of the donor star, or to a super-orbital period, or just stochastic variability. In engineering terms, the radiatively driven wind acts as a proportional controller on $\dot{M}_a(t)$, with a lag time of the order of the viscous time-scale. The set point is a luminosity slightly below the threshold for the hard-to-soft transition. If the gain of the proportional controller is sufficiently high, the lag time

inevitably causes oscillations. In earlier cycles, when the oscillating error was high enough, the system underwent a state transition.

ACKNOWLEDGEMENTS

REFERENCES

Armas Padilla M., Wijnands R., Degenaar N., Muñoz-Darias T., Casares J., Fender R. P., 2014, MNRAS, 444, 902
Arnaud K. A., 1996, in Jacoby G. H., Barnes J., eds, ASP Conf. Ser. Vol. 101, Astronomical Data Analysis Software and Systems V. Astron. Soc. Pac., San Francisco, p. 17
Artymowicz P., Lubow S. H., 1994, ApJ, 421, 651
Artymowicz P., Lubow S. H., 1996, ApJ, 467, L77
Atapin K., Fabrika S., Medvedev A., Vinokurov A., 2015, MNRAS, 446, 893
Bachetti M., 2016, Astron. Nachr., 337, 349
Begelman M. C., McKee C. F., Shields G. A., 1983, ApJ, 271, 70
Blackburn J. K., 1995, in Shaw R. A., Payne H. E., Hayes J. J. E., eds, ASP Conf. Ser. Vol. 77, Astronomical Data Analysis Software and Systems IV. Astron. Soc. Pac., San Francisco, p. 367
Blundell K. M., Bowler M. G., Schmidtobreick L., 2008, ApJ, 678, L47
Bowler M. G., 2013, A&A, 556, 149
Boyajian T. S. et al., 2012, ApJ, 757, 112
Caputo D. P., de Vries N., Patruno A., Portegies Zwart S., 2017, MNRAS, 468, 4000
Chen W., Shrader C. R., Livio M., 1997, ApJ, 491, 312
Cherepashchuk A. M. et al., 2007, in Grebenev S. et al., eds, Proc. 6th Integral Workshop, SP-622: The Obscured Universe. ESA, Noordwijk, p. 319
Conroy C., Spergel D. N., 2011, ApJ, 726, 36
Copperwheat C., Cropper M., Soria R., Wu K., 2005, MNRAS, 362, 79
Copperwheat C., Cropper M., Soria R., Wu K., 2007, MNRAS, 367, 1407
Cseh D. et al., 2015, MNRAS, 446, 3268
D'Orazio D. J., Haiman Z., MacFadyen A., 2013, MNRAS, 436, 2997
D'Orazio D. J., Haiman Z., Duffell P., MacFadyen A., Farris B., 2016, MNRAS, 459, 2379
Davis S. W., Narayan R., Zhu Y., Barret D., Farrell S. A., Godet O., Servillat M., Webb N. A., 2011, ApJ, 734, 111
de Jong J. A., van Paradijs J., Augusteijn T., 1996, A&A, 314, 484

Díaz-Trigo M., Boirin L., 2016, Astron. Nachr., 337, 368
Dubus G., Lasota J.-P., Hameury J.-M., Charles P., 1999, MNRAS, 303, 139
Dubus G., Hameury J.-M., Lasota J.-P., 2001, A&A, 373, 251
Dudik R. P., Berghea C. T., Roberts T. P., Gris e F., Singh A., Pagano R., Winter L. M., 2016, ApJ, 831, 88
Eggleton P. P., 1983, ApJ, 268, 368
Evans P. A. et al., 2009, MNRAS, 397, 1177
Fabrika S., Ueda Y., Vinokurov A., Sholukhova O., Shidatsu M., 2015, Nat. Phys., 11, 551
Farrell S. A., Sood R. K., O'Neill P. M., 2006, MNRAS, 367, 1457
Farrell S. A., Barret D., Skinner G. K., 2009a, MNRAS, 393, 139
Farrell S. A., Webb N. A., Barret D., Godet O., Rodrigues J. M., 2009b, Nature, 460, 73
Farrell S. A. et al., 2012, ApJ, 747, L13
Farrell S. A. et al., 2014, MNRAS, 437, 1208
Farris B. D., Duffell P., MacFadyen A. I., Haiman Z., 2014, ApJ, 783, 134
Farris B. D., Duffell P., MacFadyen A. I., Haiman Z., 2015, MNRAS, 446, L36
Fender R. P., Belloni T. M., Gallo E., 2004, MNRAS, 355, 1105
Feng H., Soria R., 2011, New Astron. Rev., 55, 166
Foster D. L., Charles P. A., Holley-Bockelmann K., 2010, ApJ, 725, 2480
Frank J., King A., Raine D. J., 2002, Accretion Power in Astrophysics. Cambridge Univ. Press, Cambridge
Gierliński M., Done C., Page K., 2008, MNRAS, 388, 753
Gierliński M., Done C., Page K., 2009, MNRAS, 392, 1106
Gies D. R., Huang W., McSwain M. V., 2002, ApJ, 578, L68
Gladstone J. C., Copperwheat C., Heinke C. O., Roberts T. P., Cartwright T. F., Levan A. J., Goad M. R., 2013, ApJS, 206, 14
Godet O. et al., 2012, ApJ, 752, 34
Godet O., Lombard J. C., Antonini F., Barret D., Webb N. A., Vingless J., Thomas M., 2014, ApJ, 793, 105
Grisé F., Kaaret P., Corbel S., Feng H., Cseh D., Tao L., 2012, ApJ, 745, 123
Grisé F., Kaaret P., Corbel S., Cseh D., Feng H., 2013, MNRAS, 433, 1023
Gürkan M. A., Freitag M., Rasio F. A., 2004, ApJ, 604, 632
Hameury J.-M., Lasota J.-P., McClintock J. E., Narayan R., 1997, ApJ, 489, 234
Hameury J.-M., Menou K., Dubus G., Lasota J.-P., Hure J.-M., 1998, MNRAS, 298, 1048
Harpaz A., Rappaport S., 1994, ApJ, 434, 283
Heida M. et al., 2014, MNRAS, 442, 1054
Homan J., Buxton M., Markoff S., Bailyn C. D., Nespoli E., Belloni T., 2005, ApJ, 624, 295
Hynes R. I., Haswell C. A., Chaty S., Shrader C. R., Cui W., 2002, MNRAS, 331, 169
Kalemci E., Dinçer T., Tomsick J. A., Buxton M. M., Bailyn C. D., Chun Y. Y., 2013, ApJ, 779, 95
Khabibullin I., Sazonov S., 2016, MNRAS, 457, 3963
Kimura M. et al., 2016, Nature, 529, 54
King A. R., Lasota J.-P., 2014, MNRAS, 444, L30
King A. R., Ritter H., 1998, MNRAS, 293, L42
King A. R., Kolb U., Szuszkiewicz E., 1997, ApJ, 488, 89
Kotani T., Kawai N., Matsuoka M., Brinkmann W., 1996, PASJ, 48, 619
Kovetz A., Prialnik D., Shara M. M., 1988, ApJ, 325, 828
Krivosheyev Y. M., Bisnovatyi-Kogan G. S., Cherepashchuk A. M., Postnov K. A., 2009, MNRAS, 394, 1674
Kubota A., Tanaka Y., Makishima K., Ueda Y., Dotani T., Inoue H., Yamaoka K., 1998, PASJ, 50, 667
Kubota K. et al., 2010, PASJ, 62, 323
Lasota J.-P., 2000, A&A, 360, 575
Lasota J.-P., 2001, New Astron. Rev., 45, 449
Lasota J.-P., 2008, New Astron. Rev., 51, 752
Lasota J.-P., Dubus G., Kruk K., 2008, A&A, 486, 523
Lasota J.-P., Alexander T., Dubus G., Barret D., Farrell S. A., Gehrels N., Godet O., Webb N. A., 2011, ApJ, 735, 89
Lasota J.-P., King A. R., Dubus G., 2015, ApJ, 801, L4
Lau R. M., Heida M., Kasliwal M. M., Walton D. J., 2017, ApJ, 838, L17
Leitherer C. et al., 1999, ApJS, 123, 3

Leitherer C., Ekström S., Meynet G., Schaerer D., Agienko K. B., Levesque E. M., 2014, ApJS, 212, 14

Li C., de Grijs R., Deng L., Geller A. M., Xin Y., Hu Y., Faucher-Giguère C.-A., 2016, Nature, 529, 502

Maccarone T. J., 2003, A&A, 409, 697

Malumuth E. M., Kriss G. A., Dixon W. V. D., Ferguson H. C., Ritchie C., 1992, AJ, 104, 495

Mapelli M., Zampieri L., Mayer L., 2012, MNRAS, 423, 1309

Mapelli M., Annibali F., Zampieri L., Soria R., 2013a, MNRAS, 433, 849

Mapelli M., Annibali F., Zampieri L., Soria R., 2013b, A&A, 559, 124

Marshall H. L., Canizares C. R., Hillwig T., Mioduszewski A., Rupen M., Schulz N. S., Nowak M., Heinz S., 2013, ApJ, 775, 75

Medvedev A., Fabrika S., 2010, MNRAS, 402, 479

Menou K., Hameury J.-M., Lasota J.-P., Narayan R., 2000, MNRAS, 314, 498

Middleton M. J., Walton D. J., Fabian A., Roberts T. P., Heil L., Pinto C., Anderson G., Sutton A., 2015, MNRAS, 454, 3134

Miller M. C., Farrell S. A., Maccarone T. J., 2014, ApJ, 788, 116

Mróz P. et al., 2016, Nature, 537, 649

Mucciarelli P., Zampieri L., Treves A., Turolla R., Falomo R., 2007, ApJ, 658, 999

Muno M. P., Mauerhan J., 2006, ApJ, 648, L135

Muñoz-Darias T. et al., 2016, Nature, 534, 75

Murray N., Chiang J., Grossman S. A., Voit G. M., 1995, ApJ, 451, 498

Narayan R., Sądowski A., Soria R., 2017, MNRAS, preprint (arXiv:1702.01158)

Neilsen J., Lee J. C., 2009, Nature, 458, 481

Paczyński B., 1971, ARA&A, 9, 183

Paczyński B., 1977, ApJ, 216, 822

Papaloizou J., Pringle J. E., 1977, MNRAS, 181, 441

Patruno A., Zampieri L., 2008, MNRAS, 386, 543

Perez M. S., Blundell K. M., 2009, MNRAS, 397, 849

Perez M. S., Blundell K. M., 2010, MNRAS, 408, 2

Phillips S. N., Podsiadlowski P., 2002, MNRAS, 337, 431

Pinto C., Middleton M. J., Fabian A. C., 2016, Nature, 533, 64

Podsiadlowski P., 1991, Nature, 350, 136

Ponti G., Fender R. P., Begelman M. C., Dunn R. J. H., Neilsen J., Coriat M., 2012, MNRAS, 422, L11

Portegies Zwart S. F., McMillan S. L. W., 2002, ApJ, 576, 899

Poutanen J., Lipunova G., Fabrika S., Butkevich A. G., Abolmasov P., 2007, MNRAS, 377, 1187

Proga D., Kallman T. R., 2002, ApJ, 565, 455

Proga D., Stone J. M., Drew J. E., 1998, MNRAS, 295, 595

Rahoui F., Chaty S., Rodriguez J., Fuchs Y., Mirabel I. F., Pooley G. G., 2010, ApJ, 715, 1191

Rana V. et al., 2016, ApJ, 821, 103

Rau A., Greiner J., McCollough M. L., 2003, ApJ, 590, L37

Rees M. J., 1988, Nature, 333, 523

Remillard R. A., McClintock J. E., 2006, ARA&A, 44, 49

Ritter H., 2008, New Astron. Rev., 51, 869

Ritter H., Zhang Z.-Y., Kolb U., 2000, A&A, 360, 969

Roedig C., Krolik J. H., Miller M. C., 2014, ApJ, 783, 134

Russell T. D., Soria R., Motch C., Pakull M. W., Torres M. A. P., Curran P. A., Jonker P. G., Miller-Jones J. C. A., 2014, MNRAS, 439, 1381

Servillat M., Farrell S. A., Lin D., Godet O., Barret D., Webb N. A., 2011, ApJ, 743, 6

Shahbaz T., Charkles P. A., King A. R., 1998, MNRAS, 301, 382

Shakura N. I., Sunyaev R. A., 1973, A&A, 24, 337

Shields G. A., McKee C. F., Lin D. N. C., Begelman M. C., 1986, ApJ, 306, 90

Soria R., 2013, MNRAS, 428, 1944

Soria R., Hau G. K. T., Graham A. W., Kong A. K. H., Kuin N. P. M, Li I.-H., Liu J.-F., Wu K., 2010, MNRAS, 405, 870

Soria R., Zampieri L., Zane S., Wu K., 2011, MNRAS, 410, 1886

Soria R., Hakala P. J., Hau G. K. T., Gladstone J. C., Kong A. K. H., 2012a, MNRAS, 420, 3599

Soria R., Kuntz K. D., Winkler P. F., Blair W. P., Long K. S., Plucinsky P. P., Whitmore B. C., 2012b, ApJ, 750, 152

Soria R., Hau G. K. T., Pakull M. W., 2013, ApJ, 768, L22

Strohmayer T. E., 2009, ApJ, 706, L210

Sutton A. D., Roberts T. P., Middleton M. J., 2013, MNRAS, 435, 1758

Sutton A. D., Done C., Roberts T. P., 2014, MNRAS, 444, 2415

Sutton A. D., Roberts T. P., Middleton M. J., 2015, ApJ, 814, 73

Tao L., Feng H., Grisé F., Kaaret P., 2011, ApJ, 737, 81

Tao L., Kaaret P., Feng H., Grisé F., 2012, ApJ, 750, 110

Urquhart R., Soria R., 2016, MNRAS, 456, 1859

van der Helm E., Portegies Zwart S., Pols O., 2016, MNRAS, 455, 462

van Paradijs J., McClintock J. E., 1994, A&A, 290, 133

Viallet M., Hameury J.-M., 2008, A&A, 489, 699

Vilhu O., Ergma E., Fedorova A., 1994, A&A, 291, 842

Vrtilek S. D., Raymond J. C., Garcia M. R., Verbunt F., Hasinger G., Kurster M., 1990, A&A, 235, 162

Warner B., 1995, Cataclysmic Variable Stars. Cambridge Univ. Press, Cambridge

Webb N. et al., 2012, Science, 337, 554

Webb N. A., Godet O., Wiersema K., Lasota J.-P., Barret D., Farrell S. A., Maccarone T. J., Servillat M., 2014, ApJ, 780, L9

Whitehurst R., 1988, MNRAS, 232, 35

Wiersema K., Farrell S. A., Webb N. A., Servillat M., Maccarone T. J., Barret D., Godet O., 2010, ApJ, 721, L102

Yan Z., Yu W., 2015, ApJ, 805, 87

Yan Z., Zhang W., Soria R., Altamirano D., Yu W., 2015, ApJ, 811, 23

Yan C.-S., Lu Y., Dai X., Yu Q., 2015, ApJ, 809, 117

This paper has been typeset from a TEX/LATEX file prepared by the author.